

Elkins Lynne J. (Orcid ID: 0000-0002-0903-7091)
Marzoli Andrea (Orcid ID: 0000-0003-0093-2759)
Bizimis Michael (Orcid ID: 0000-0002-4611-6928)

Assessing origins of end-Triassic tholeiites from Eastern North America using hafnium isotopes

Lynne J. Elkins^{1, *}, Christine M. Meyzen², Sara Callegaro³, Andrea Marzoli², Michael Bizimis⁴

¹ University of Nebraska-Lincoln, Lincoln, NE 68510; lelkins@unl.edu

² Dipartimento di Geoscienze, Università degli Studi di Padova, Via G. Gradenigo, 6, 35131 Padova, Italy; andrea.marzoli@unipd.it, christine.meyzen@unipd.it

³ Centre for Earth Evolution and Dynamics, University of Oslo, Oslo, Norway; sara.callegaro@geo.uio.no

⁴ University of South Carolina; mbizimis@geol.sc.edu

* Corresponding author: Lynne Elkins (lelkins@unl.edu)

Key Points:

- End-Triassic tholeiites from Eastern North America were likely products of melting Paleozoic age, subduction-metasomatized mantle
- Direct melting of recycled crustal rocks may also have occurred, but cannot fully explain the tholeiite isotopic compositions observed
- Southern Eastern North American tholeiites likely also experienced assimilation of lower continental crust, possibly intermediate granulite

This article has been accepted for publication and undergone full peer review but has not been through the copyediting, typesetting, pagination and proofreading process which may lead to differences between this version and the Version of Record. Please cite this article as doi: 10.1029/2020GC008999

Abstract

The driving processes responsible for producing the Central Atlantic Magmatic Province, the Large Igneous Province associated with end-Triassic rifting of Pangea, remain largely debated. Because their compositions encompass most of the Central Atlantic basalt spectrum, tholeiites from southern Eastern North America are considered pivotal for identifying magma origins. New $^{176}\text{Hf}/^{177}\text{Hf}$ measurements for 201 Ma Eastern North American tholeiites dominantly record a local petrogenetic history. Their ϵ_{Hf} ratios, corrected to an emplacement age of 201 Ma (-7.85 to +5.86), form a positive but shallowly sloped array slightly deviating from the terrestrial array on a ϵ_{Hf} vs. ϵ_{Nd} diagram. Comparison of $^{176}\text{Hf}/^{177}\text{Hf}$ to other isotope ratios and trace elements helps to rule out several petrogenetic scenarios, particularly mixing of melts from global depleted or enriched mantle components. In contrast, partial melting of subduction-metasomatized mantle can explain the parental magma composition for southern Eastern North America. Such metasomatism likely occurred during Paleozoic subduction around Pangea and may have been dominated by sediment-derived fluid reactions. The observed $^{176}\text{Hf}/^{177}\text{Hf}$ vs. $^{143}\text{Nd}/^{144}\text{Nd}$ array may reflect subsequent assimilation of lower continental crust, perhaps together with limited direct melting of recycled continental crust in the asthenosphere. The proposed recycling scenario does not specifically support or preclude a mantle plume origin for the Central Atlantic Magmatic Province, but instead points toward the presence of a distinct local mantle source and crustal assimilation processes during magma transport. Detailed understanding of these local effects is needed in order to more accurately understand the origins of Large Igneous Provinces.

Key words: 8410 Geochemical modeling; 8137 Hotspots, large igneous provinces, and flood basalt volcanism; 1040 Radiogenic isotope geochemistry; 1037 Magma genesis and partial melting

1. INTRODUCTION

The Triassic-Jurassic rifting of Pangea and subsequent opening of the central Atlantic Ocean represent a major stage of a Wilson cycle, describing the formation and destruction of oceanic basins and supercontinents (Wilson, 1966). Wilson's classic model drew directly on the central Atlantic basin and its history of repeated closures and reopenings as a primary example of global tectonic processes. End-Triassic rifting was associated with the emplacement of one of the most voluminous continental flood basalt provinces in Earth history (Figure 1), the Central Atlantic Magmatic Province (CAMP; Marzoli et al., 1999), an event significant enough to have likely triggered the end-Triassic mass extinction (Capriolo et al., 2020; Cirilli et al., 2009; Davies et al., 2017; Heimdal et al., 2018; Hesselbo et al., 2002; Marzoli et al., 2004). Major continental rifting events in geologic history are commonly associated with the eruption of a large igneous province (LIP), but the causal relationships linking rifts with LIPs remain unclear. The distinction and the transition between passive and active rifting models has been the object of several studies (Burov & Gerya, 2014; Courtillot et al., 1999; Koptev et al., 2015; Sengör & Burke, 1978), all seeking to better understand what processes initiate rifting and what factors cause rifted margins to be magma-rich or magma-poor (Gillard et al., 2017). Large igneous provinces may also record the arrival of deep-seated mantle plumes at the base of the lithosphere, which could in turn act to initiate rifting, but it has been difficult to fully reconcile plume head arrival with continental rifting models in all settings (e.g., Carlson, 1991; Courtillot et al., 1999; Morgan, 1983; Saunders et al., 2007).

One peculiarity of CAMP magmas is that they display an overall high degree of geochemical heterogeneity, which has led researchers to propose diverse magma origins such as an upwelling mantle plume (e.g., Cebriá et al., 2003; De Boer, 1992; Oyarzun et al., 1997; Wilson, 1997); metasomatized subcontinental lithospheric mantle (SCLM) (e.g., Deckart et al., 2005; Merle et al., 2011; Verati et al., 2005); and asthenosphere and/or SCLM modified by

subduction-derived materials (e.g., Alibert, 1985; Callegaro et al., 2013, 2017; Dorais et al., 2005; Dupuy et al., 1988; Heatherington & Mueller, 1999; Marzoli et al., 2019; Merle et al., 2014; Pegram, 1990; Whalen et al., 2015). These proposed origins have been likewise interpreted to indicate various geodynamic scenarios (e.g., Marzoli et al., 2018, and references therein). As an additional source of complexity, while some of the diverse magma types have been identified across the province, other CAMP magma compositions vary from region to region (Marzoli et al., 2018). It remains unclear whether these regional heterogeneities are derived from locally diverse asthenospheric or continental lithospheric mantle sources, or inherited by assimilation of local continental lithosphere by deeper, perhaps plume-derived primary magmas. Each scenario has distinct implications for how end-Triassic rifting and associated LIP emplacement occurred. The diversity of models further demonstrates the uncertainty about the origins of LIPs and their links to continental rifts.

As an important component of this ongoing effort to understand the origins of CAMP, much prior literature has been dedicated to the petrogenesis of CAMP basalts from Eastern North America (ENA), but questions persist about the characteristics and origins of their primary melt sources, and the role and importance of assimilation and crustal contamination in modifying primitive melt compositions (e.g., Callegaro et al., 2013; Dorais & Tubrett, 2008; Dostal and Dupuy, 1984; Dostal & Durning, 1998; Heatherington & Mueller, 1999; McHone, 2000; Merle et al., 2014; Pegram, 1990; Puffer, 1992, 2001, 2003; Shellnutt et al., 2018; Tollo & Gottfried, 1992; Whalen et al., 2015). Because of the geochemical heterogeneity recorded by the tholeiites from Georgia to Virginia in the southern part of ENA, which encompass most of the CAMP geochemical spectrum, and taking advantage of the mineralogical sensitivity of the ^{176}Lu - ^{176}Hf isotopic system with respect to clinopyroxene-garnet ratios, this study aims to place new constraints on the formation of CAMP and of LIPs more generally.

2. GEOLOGIC SETTING

2.1. Tectonic setting of CAMP

The opening of the Central Atlantic oceanic basin started with end-Triassic rifting of the supercontinent Pangea, an event associated with the regional emplacement of tholeiitic magmas over an estimated total surface of 10^7 km² spanning present-day eastern North America, northern South America, northwest Africa, and southwestern Europe (Figure 1) (Marzoli et al., 1999, 2018). Central Atlantic Magmatic Province emplacement occurred at ~201 Ma with a duration of peak magmatic activity constrained to less than 0.6 Ma (e.g., Blackburn et al., 2013; Davies et al., 2017; Deckart et al., 1997; Dunning & Hodych, 1990; Hames et al., 2000; Hodych & Dunning, 1992; Jourdan et al., 2009; Knight et al., 2004; Marzoli et al., 2004, 2011, 2019; Nomade et al., 2007; Sebai et al., 1991; Verati et al., 2005, 2007). At ca. 201.6 to 200.9 Ma, several short-lived magmatic pulses occurred all over the CAMP and preceded continental break-up by several million years (Blackburn et al., 2013; Davies et al., 2017; Knight et al., 2004).

2.2. Models for CAMP formation

The origins of LIPs and their relationship with continental rifting are subjects of long standing debate (e.g., Bryan & Ernst, 2008; Carlson, 1991; Coffin & Eldholm, 1992; Kent, 1991; Morgan, 1983; Saunders et al., 2007). Many studies have invoked one or more mantle plumes as triggering mechanisms for CAMP rifting and magmatism, invoking heat-driven lithospheric erosion and thinning, wide-scale asthenospheric upwelling and melting in a plume head, broad crustal magmatic emplacement, and possible localized focusing of regional extension in response to plume impingement on the overlying plate (e.g., Cebriá et al., 2003; Hill, 1991; Lizarralde & Holbrook, 1997; McHone, 1978; Morgan, 1983; Oyarzun et al., 1997; Ruiz-Martínez et al., 2012; White & McKenzie, 1989; Wilson, 1997).

However, plume evidence related to the CAMP episode is ambiguous: the central Atlantic basin does not include any hotspot tracks of early Jurassic age, and dike orientations and the near-synchronous onset of magmatism from Bolivia to Spain are inconsistent with a centralized, radiating plume impact (e.g., Davies et al., 2017; May, 1971; McHone, 2000; Verati et al., 2005). Therefore, many studies have advocated for non-plume dynamical mechanisms for triggering rifting and melting (e.g., Bédard, 1992; De Min et al., 2003; Holbrook & Kelemen, 1993; Holbrook et al., 1994; Kontak, 2008; McHone, 2000). These alternative models for CAMP invoke other melt generation mechanisms, such as subcontinental insulation heating and edge-driven convection (e.g., Anderson, 1994; Coltice et al., 2007).

Geochemically, most CAMP magmas exhibit signatures enriched in incompatible trace elements, with combined Pb-Sr-Nd-Os radiogenic isotopes indicating the involvement of one or more long-lived source reservoirs with time-integrated incompatible trace element enrichment (e.g., Callegaro et al., 2013, 2014, 2017; Marzoli et al., 2019; Merle et al., 2011, 2014; Whalen et al., 2015). While these geochemical patterns could indicate melt contributions from recycled material entrained in a deep mantle plume, geochemical signatures such as LILE enrichments and Nb depletions in CAMP are notably arc-like (e.g., De Min et al., 2003; Deckart et al., 2005; Jourdan et al., 2003; Puffer, 2001).

The arc-like trace element signatures observed in CAMP magmas could indicate a unique local mantle source composition, or may be derived from assimilation of continental lithosphere during magma transport (Alibert, 1985; Bertrand, 1991; Bertrand et al., 1982; Cebriá et al., 2003; Chabou et al., 2010; De Min et al., 2003; Deckart et al., 2005; Dupuy et al., 1988; Heatherington & Mueller, 1999; Iacumin et al., 2003; Jourdan et al., 2003; Papezik et al., 1988; Pegram, 1990; Puffer, 1992; Ragland et al., 1992; Tollo & Gottfried, 1992; Verati et al., 2005).

A plume origin for the Sr-Nd-Pb isotope systematics of CAMP is likewise problematic given the lack of Atlantic OIBs with comparable signatures (e.g., Janney & Castillo, 2001; Pegram, 1990). A lack of primitive (picritic) magmas in CAMP is a hindrance when defining the mantle source origins for the LIP, but recent isotope analyses of ENA tholeiites suggest that for the least evolved magmas, a SCLM or shallow asthenospheric mantle source modified by either subduction-derived fluids or direct addition of subducted and/or delaminated continental crustal material is a viable scenario (Callegaro et al., 2013, 2014; Merle et al., 2014; Shelnutt et al., 2018; Whalen et al., 2015).

2.3. The Eastern North America study area

Eastern North American CAMP (Figure 1) hosts a particularly well-documented volcanic and intrusive tholeiite series, including dike swarms, sills, and basaltic flows exposed from Georgia (USA) to Newfoundland (Canada). The ENA series incorporate much of the observed geochemical diversity of the overall province. The major CAMP lava piles are locally associated with extensional grabens and half-grabens along what is now eastern North America. The Hartford-Newark-Gettysburg-Culpeper basins of Massachusetts, Connecticut, New Jersey, Pennsylvania, and Virginia host a series of three major volcanic episodes, including the oldest Orange Mountain series, the intermediate-age Preakness series, and the youngest Hook Mountain series (e.g., Puffer, 1992; Tollo & Gottfried, 1992). These units are matched by similarly dated and geochemically identified basalts and feeder dikes in Canada (e.g., Kontak, 2008; Jourdan et al., 2009; Pe-Piper & Piper, 1999) and Morocco (e.g., Bertrand et al., 1982; Marzoli et al., 2019). Contrary to observations in Morocco and northern ENA, rift basins in southern Virginia, the Carolinas, and Georgia do not preserve lava flows and are dominated instead by diabase dikes and a few sills (e.g., Ragland et al., 1992; Weigand & Ragland, 1970).

Diabases and basalt flows from ENA are geochemically diverse, and detailed analysis has indicated that multiple parental magmas with distinct differentiation, fractionation, and/or assimilation paths are likely necessary to generate the geochemical variations observed (e.g., Tollo & Gottfried, 1992). Mantle potential temperatures extrapolated from high-Fo ($> F_{0.87}$) olivine cores from these rocks have a maximum calculated value of 1480°C (Callegaro et al., 2013; Herzberg & Gazel, 2009; Hole, 2015), well below anomalously high temperatures calculated for the likely plume-related Deccan and Siberian LIPs, but at least 100 °C higher than normal ambient upper mantle (Herzberg & Gazel, 2009; Sobolev et al., 2011). These moderately high temperatures raise questions about the origins of that heat in the absence of a mantle plume; one possibility is continental insulation beneath supercontinents (e.g., Coltice et al., 2007; Rey, 2015). Within this framework, the wide geochemical variability observed in ENA tholeiitic dikes and sills makes it a particularly good focus region for placing new geochemical constraints on the diversity of magma source origins and the process of continental flood basalt production during rifting.

2. METHODS

2.1. CAMP sample selection and preparation

Tholeiitic basalt and diabase samples were selected to achieve a representative coverage across the geochemical variability observed in trace elements and Sr-Nd-Pb isotopes for the southern ENA region (12 samples), as well as targeted comparison to other regions within CAMP including the northern ENA Newark basin (six samples), Sierra Leone (one sample), and Morocco (one sample) (Table 1, Figure 1). The selected samples have relatively fresh, unaltered appearances, with prior major and trace element results indicative of minimal crustal assimilation or post-eruptive alteration (Callegaro et al., 2013, 2017; Marzoli et al., 2019; Merle et al., 2014). Of these, two southern ENA samples (CS28 and CS57) were selected

because they are particularly Mg-rich (> 12 wt.% MgO) and are among the most primitive rocks ever recovered from CAMP (Table 1; Callegaro et al., 2013). An exception to the above criteria is sample NEW68 from the Preakness unit of the Newark Basin, which was selected because it is likely crustally contaminated (Merle et al., 2014).

The samples analyzed for this study were all collected during prior research, and sampling locations and previous geochemical measurements have been published elsewhere (Callegaro et al., 2013, 2017; Marzoli et al., 2019; Merle et al., 2014) (Table 1). Prior to analysis for the current study, any weathered rinds were removed by cutting with a trim saw. Fresh, visibly unaltered material was then broken into finer pieces using a rock hammer, which was protected with layers of clean plastic sheeting to prevent contamination. Sample material was then reduced to small chips and powdered using an agate mortar and pestle. Larger samples with a sufficient volume of material were further powdered using a Spex Shatterbox alumina grinding apparatus. Samples were prepared in this manner either at the University of Padova or at the University of Nebraska-Lincoln.

2.2. Analytical methods

Samples were analyzed for Hf isotopes in the Center for Elemental Mass Spectrometry, School of Earth, Ocean, and Environment, University of South Carolina. An aliquot of 100 mg of rock powder was weighed and digested in a Teflon-distilled HF:HNO₃ mixture in a 3:1 ratio. After dissolution, the solution was dried repeatedly in 6N HCl, after which Hf was separated from matrix elements using Eichrom LN-Spec Resin and methods after Munker et al. (2001). Hafnium separates were analyzed by mass spectrometry methods using a Thermo Neptune multi-collector inductively-coupled plasma mass spectrometer (MC-ICP-MS). Procedural blanks recorded Hf concentrations under 50 pg, and analytical precision was within 0.0017% (2σ standard error) for all measured samples (Table 2). Isotope compositions were corrected

for mass fractionation using $^{179}\text{Hf}/^{177}\text{Hf} = 0.7325$. The JMC-475 standard was determined to have $^{176}\text{Hf}/^{177}\text{Hf} = 0.282152 \pm 0.000004$ ($n = 10$) for the first round of analyses and $^{176}\text{Hf}/^{177}\text{Hf} = 0.282142 \pm 0.000007$ ($n = 10$) for the second batch (Table 2). The data were corrected for instrumental bias using a JMC-475 reference value of 0.282160. As an additional test of external reproducibility, we analyzed a gabbroic sample from the Freetown Layered Complex (Sierra Leone) as a replicate of an earlier measurement by Callegaro et al. (2017), using a separate dissolution. Our newly measured $^{176}\text{Hf}/^{177}\text{Hf}$ ratio for this sample (0.282917 ± 0.000005 ; Table 2) is similar to the prior published result (0.282937 ± 0.000012). The two results are slightly outside of 2σ uncertainty with each other, however, which may be attributed to minor sample heterogeneity and the measurement of separate sample dissolutions. Additional analytical details and standard information can be found in Khanna et al. (2014), Mallick et al. (2015), and Frisby et al. (2016).

3. RESULTS

All data measured in this study have been age corrected to a crystallization age of 201 Ma using Lu/Hf ratios previously published for these samples (Callegaro et al., 2013, 2017; Marzoli et al., 2019; Merle et al., 2014) (Table 2); age-corrected isotopic ratios are hereafter indicated with “201 Ma” notation. A conservative uncertainty of ~5% for the Lu/Hf ratio translates to less than 0.3 ϵ_{Hf} units of uncertainty in the initial isotopic composition for rocks of this age, and has no effect on the conclusions of this study. Most samples from the southern ENA region form a distinct array exhibiting a shallower slope (slope = 0.92 ± 0.12) than the terrestrial array (Vervoort et al., 2011), being slightly shifted toward higher $\epsilon_{\text{Hf} 201\text{Ma}}$ ratios for a given $\epsilon_{\text{Nd} 201\text{Ma}}$ value (Table 2, Figure 2a). A notable exception is sample CS73 from Virginia, which plots along the terrestrial array. The oblique trend relative to the terrestrial array defined by southern ENA samples resembles trends previously observed for basalts from Hawaii (Blichert-Toft et

al., 1999; Salters et al., 2006) and the Karoo LIP (Jourdan et al., 2007) (Figure 2a). Southern ENA $\epsilon_{\text{Hf}}^{201\text{Ma}}$ ratios also form a slightly positive correlation with $^{206}\text{Pb}/^{204}\text{Pb}_{201\text{Ma}}$ isotope ratios (Callegaro et al., 2013) (Figure 2b). The latitudinal $\epsilon_{\text{Hf}}^{201\text{Ma}}$ profile between 34 and 37 °N shows a decreasing southward gradient (Figure S1) toward more enriched (less radiogenic) isotope ratios, with the exception of sample CS73.

In contrast with ENA samples, those from the Newark basin, Morocco, and Sierra Leone are overall consistent with the global array (Vervoort et al., 2011) (Figure 2a). An exception is the sample NEW68, a Preakness unit tholeiite selected for comparison due to its distinct geochemical signature indicative of crustal assimilation (Merle et al., 2014); NEW68 has a slightly higher $\epsilon_{\text{Hf}}^{201\text{Ma}}$ ratio for its $\epsilon_{\text{Nd}}^{201\text{Ma}}$ than other Newark basin basalts. Newark basin samples exhibit a range of $\epsilon_{\text{Hf}}^{201\text{Ma}}$ values from ~0 to +5 (Figure S1).

4. DISCUSSION

The shallow slope of southern ENA tholeiites relative to the terrestrial array (Figure 2a, Table 2) indicates a systematically increasing contribution from a low- ϵ_{Hf} source towards the south (Figure S1). However, unlike previous data sets such as Hawaiian basalts (Blichert-Toft et al., 1999; Salters et al., 2006) and the Karoo LIP (Jourdan et al., 2007), the southern ENA CAMP array extends towards low $^{206}\text{Pb}/^{204}\text{Pb}_{201\text{Ma}}$ ratios at the low- $\epsilon_{\text{Nd}}^{201\text{Ma}}$ end of the array (Figure 2). Below, we explore a series of melt mixing and assimilation scenarios and compare the outcomes to the observed CAMP trace element and isotopic data, in an attempt to explain the origins of these isotopic characteristics.

4.1. Crustal assimilation in Carolina tholeiites

As noted above, aside from a few samples, recent isotopic studies of ENA and other CAMP rocks have indicated relatively minor crustal assimilation effects (up to 10% assimilation) in

ENA tholeiites (Callegaro et al., 2013; Merle et al., 2014; Whalen et al., 2015), which have relatively low age-corrected $^{187}\text{Os}/^{188}\text{Os}_{201\text{Ma}}$ (0.128 – 0.187, mean 0.137) despite high $^{87}\text{Sr}/^{86}\text{Sr}_{201\text{Ma}}$ (0.70438 - 0.71074, mean 0.70613), high $^{207}\text{Pb}/^{204}\text{Pb}_{201\text{Ma}}$ (15.54 - 15.67, mean 15.61), variable $^{206}\text{Pb}/^{204}\text{Pb}_{201\text{Ma}}$ (17.41 - 18.65, mean 18.23), and low $^{143}\text{Nd}/^{144}\text{Nd}_{201\text{Ma}}$ ratios (0.51204 - 0.51251, mean 0.51230). However, due to a lack of Hf compositional and isotopic data for the potential end-member continental assimilants in the ENA province, it is unclear what effects up to 10% crustal assimilation may have had on the Hf isotope compositions of ENA CAMP magmas. To evaluate the potential impacts of assimilation on the Hf data set, we calculated the effects of assimilation-fractional crystallization on ENA basalts using energy-constrained methods after Bohrsen and Spera (2001) and Spera and Bohrsen (2001) (Tables S1, S2; Figure 3), and considered three potential assimilants: local upper continental crust, and both mafic and intermediate-SiO₂, lower crustal granulite rocks. To simplify the scenarios tested, we make several initial assumptions, including the temperatures, compositions, and energy properties of the primary magma and three assimilants (see Tables S1, S2). Our calculations also assume a primary magma composition resembling the most incompatible element-depleted, southern ENA tholeiite measured in this study with respect to Hf (sample CS49, with low [Hf] = 1.3 ppm, high $\epsilon_{\text{Hf} 201\text{Ma}} = +5.86$) (Table 2).

To estimate the average composition of local upper continental crust, we used the mean compositions of measured Carolina terrane crustal rocks from Pettingill et al. (1984) and Sinha et al. (1996) and the data compilation of Whalen et al. (2015) (Table S1). The composition and age of the lower basement of the Carolina terrane is less well-constrained. In general, while some lower continental crust (LCC) may be Phanerozoic in age, many lower crustal rocks worldwide are composed of Archean to Proterozoic Precambrian granulites with a range of mafic to felsic compositions (e.g., Huang et al., 1995; Schmitz et al., 2004; Vervoort et al., 2000), and there is isotopic evidence that local Carolina terrane LCC is dominantly Proterozoic

in age (Ingle et al., 2003). While a range of LCC ages is thus possible, here we focus on Proterozoic lower crustal sources for the Carolina terrane. Most lower crustal granulites measured lie along the terrestrial ϵ_{Nd} - ϵ_{Hf} array (Vervoort et al., 2000), but some granulite xenoliths exhibit decoupling of ϵ_{Hf} from ϵ_{Nd} , likely caused by the presence of cumulate or restite igneous minerals or by fractionation during metamorphic mineral growth (Schmitz et al., 2004). The decoupling toward higher ϵ_{Hf} relative to the terrestrial array is primarily observed in Proterozoic granulites (Huang et al., 1995; Schmitz et al., 2004; Zartman et al., 2013), and so also may play a role in the Carolina terrane (Ingle et al., 2003). As for major element compositions, while much of the LCC may be mafic, Zhao and Guo (2019) and Guo et al. (2019) have observed that local Carolina LCC likely has an overall intermediate SiO_2 content; we thus test both mafic and intermediate- SiO_2 LCC compositions (Figure 3, Table S1). The mafic LCC composition used here resembles mafic granulite xenoliths from Michigan (Zartman et al., 2013) with decoupled ϵ_{Hf} and ϵ_{Nd} ; alternative assimilation trajectories for mafic granulites lying along the terrestrial array exhibited a poorer fit and, for simplicity, are not shown. We assume that the intermediate granulite has comparatively enriched (unradiogenic) Hf and Nd isotopes and resembles intermediate- SiO_2 granulite xenoliths from South Africa and measured by Schmitz et al. (2004) (Table S1). Several Pb isotopic compositions were tested for the LCC assimilation scenarios to determine the best fit to the measured ENA CAMP data set (see Figure 3, Table S1, S2), considering the large span of Pb isotopic ratios exhibited by the basement terranes previously accreted to ENA (Pettingill et al., 1984; Sinha et al., 1996; Whalen et al., 2015). Because well-characterized intermediate- SiO_2 granulite xenoliths in the literature are largely peraluminous, a composition that may not be representative of all lower crust, we further tested a more aluminum-poor composition based on well-characterized, intermediate- SiO_2 granulites from Jonsa, Finland (Nehring et al., 2010); however, the Finnish

granulite composition likewise exhibited a poorer fit than the other results, so for simplicity it is not shown.

We show our calculated crustal assimilation trajectories in Figure 3. Only the relatively enriched, intermediate-SiO₂ granulite assimilant can account for most of the Hf-Nd isotopic variability observed in our samples with 10% assimilation or less (Figure 3). Up to 10% assimilation of Carolina terrane UCC rocks cannot explain most of the $\epsilon_{\text{Hf}}-\epsilon_{\text{Nd}}$ data array (Figure 3). Mafic LCC assimilation trajectories deviate to much higher ϵ_{Hf} than our sample data (Figure 3) when using the isotopically decoupled assimilant after Zartman et al. (2013), and none of the mafic granulite Pb isotope compositions tested are able to explain our samples' Pb isotopes using only 10% addition (see also Callegaro et al., 2013; Merle et al., 2014; Whalen et al., 2015). For intermediate-SiO₂ LCC, the Pb isotope composition of an assimilant needs to be relatively unradiogenic (e.g., $^{206}\text{Pb}/^{204}\text{Pb} \sim 17.0-17.3$), but the assimilant must also have relatively unradiogenic $^{176}\text{Hf}/^{177}\text{Hf}$ and $^{143}\text{Nd}/^{144}\text{Nd}$ compositions (Figure 3). Such a low $^{206}\text{Pb}/^{204}\text{Pb}$ composition may be plausible when compared with the ranges measured in granulites from Antarctica (Wysoczanski et al., 1995), Scotland (Halliday et al., 1993), and Michigan (Zartman et al., 2013), which provide global examples of intermediate to felsic lower crustal granulites, and also in light of the low $^{206}\text{Pb}/^{204}\text{Pb}$ signatures observed in some exposed Carolina terrane rocks (granulites, charnockites, and anorthosites; Sinha et al., 1996).

All of our LCC assimilation calculations exhibit concave-down curvature in Figure 3, suggesting that, e.g., Pb may generally be more significantly impacted than Hf by assimilation processes because of its higher concentrations in granulitic basement relative to mantle-derived basalts (e.g., Zartman et al., 2013). We further note that among our tested compositions, only a crustal contaminant containing accessory zircon, like our intermediate-SiO₂ granulite composition, had sufficiently high Hf partition coefficients to reproduce the isotope

compositions observed in our southern ENA data set with only 10% assimilation. In our calculations, the presence of minor zircon in the assimilant rock also extends the compositions of magmas experiencing even minor assimilation to more highly unradiogenic ϵ_{Hf} values (Figure 3). The role of accessory minerals in magma assimilation processes is, however, presently unclear and likely to be more complex than our models allow. For example, minerals like zircon may be effectively dissolved from country rocks adjacent to mafic sills and dikes early in the melt-rock interaction process, depending on local zircon abundance, grain size, and Zr saturation in the melt (e.g., Bindeman & Melnik, 2016). Melt-rock interaction between intruding magmas and granulitic country rocks is also likely to be highly variable both spatially and over time, beyond the relatively simple calculated scenarios shown in Figure 3. We thus only conclude that limited absorption of intermediate-SiO₂, relatively isotopically enriched granulitic wallrock by primary CAMP tholeiitic magmas may in part account for elevation of southern ENA samples above the terrestrial data array, within the 10% assimilation constraint previously identified using Os isotopes (Callegaro et al., 2013; Merle et al., 2014).

4.2. Source origins of Eastern North American tholeiites

While assimilation of crust may play a role in generating part of the isotopic variability observed, some observations, such as the complex Pb isotope systematics, still favor additional mantle source heterogeneity effects to fully explain the origins of ENA CAMP (Callegaro et al., 2013; Merle et al., 2014; Whalen et al., 2015). Based on their distribution, much of the isotopic variations observed in ENA CAMP tholeiite samples may require the involvement of multiple distinct mantle sources (Figure 2). Below we explore current working hypotheses for heterogeneous source origins of the southern ENA CAMP data set, including 1) global mantle reservoirs, 2) SCLM, and 3) recently recycled crust in the local asthenosphere.

4.2.1. Hypothesis 1: Global mantle reservoirs as a source for CAMP

A technique for identifying possible plume-derived and/or long-lived mantle reservoirs for the central Atlantic region is considering the end member basalt compositions observed in local ocean island basalts, such as the Azores (Béguelin et al., 2017), Madeira (Geldmacher et al., 2011), or Bermuda (Mazza et al., 2019), as well as Mesozoic MORB (Janney & Castillo, 2001) and recently identified Eocene magmatism in the Appalachians (Mazza et al., 2017) (Figure 2). However, prior research (e.g., Marzoli et al., 2019, and references therein) has consistently shown that such end-members cannot explain all of the isotopic compositions observed in CAMP, and indeed Atlantic intraplate basalts span a notably different compositional range than that observed across the ENA CAMP data set.

Long-lived mantle components, such as depleted MORB mantle (DMM) and the most extreme enriched mantle end-members (EM-1 and EM-2), define a broader range of isotopic compositions, and their potential contribution in generating the observed trends in CAMP compositions is examined here. This scenario resembles the proposed origin for many hotspot volcanic centers and ocean islands, and would potentially suggest the presence in the melt zone of materials transported from the deep mantle via a mantle plume. However, recent isotope measurements of ENA CAMP have demonstrated that mixing of long-lived, global mantle components in a heterogeneous mantle source is unable to fully explain the range of isotope compositions observed, particularly for Pb isotope ratios (Callegaro et al., 2013, 2014, 2017; Merle et al., 2011, 2014), and that outcome remains unchanged by our new Hf contributions as demonstrated by our mixing calculations (Figures 4, 5). In those calculations, we test more recent estimates for the isotopic compositions of EM-1 and EM-2 (e.g., Jackson and Dasgupta, 2008; Jackson et al., 2007; Table S1), which have less extreme Pb isotope compositions than, e.g., earlier estimates that were used in prior CAMP studies (e.g., Whalen et al., 2015); our

results do not, however, achieve a better fit to ENA CAMP isotopic data than previous work. We further note that while parts of our data set resemble partial melts of enriched mantle reservoirs like EM-1 or EM-2, the trend of the southern ENA CAMP data array is inconsistent with the sense of enrichment implied by mixing trajectories in Figures 4 and 5. In particular, the samples with isotopic signatures towards the low- ϵ_{Hf} end of the data array (i.e., trending towards enriched mantle) also exhibit relatively low Pb isotope ratios and thus appear to trend away from the same end members in Pb-isotope space. This apparent mismatch indicates that additional partial melt sources must be considered to fully explain the origins of southern ENA CAMP.

4.2.2. Hypothesis 2: Melting of subcontinental lithospheric mantle

It is possible that the lithospheric mantle beneath CAMP has experienced prior melting (e.g., during rifting of Laurussia) that may have left a depleted and refractory lithospheric mantle residue. The moderately high temperatures calculated for CAMP (Herzberg & Gazel, 2009) may have then been sufficient to cause melting of the refractory SCLM: at temperatures of 1480°C and relatively low mantle pressures (1.5-2.0 GPa), Falloon and Danyushevsky (2000) predicted 6-12% melting of anhydrous harzburgite. This refractory mantle should be depleted in incompatible trace elements and thus may resemble depleted asthenospheric mantle in trace element and isotopic composition, making it difficult to uniquely identify. We note that in this scenario, heating and melting of refractory lithosphere would need to be sufficiently widespread to explain the large volume of magma likely deposited during CAMP. The total volume emplaced remains unknown, but the province spans a total area of approximately 10^7 km², as noted above. We further note that mantle temperatures sufficient to remelt refractory SCLM are also sufficient to melt the more fertile underlying lherzolitic asthenosphere, and the geochemical signatures of these two scenarios are expected to significantly overlap. Such

asthenospheric melting is likely to produce an additional volume of magma that would overwhelm the trace element contribution from the less fertile, trace element depleted, harzburgitic lithospheric rocks.

On the other hand, supra-subduction zone SCLM, such as that produced during the assembly of Pangea, is further expected to be variably infiltrated by metasomatic fluids that would impart a more enriched trace element and isotopic composition. A metasomatized SCLM is thus an alternative and more fertile melt source that has been suggested for CAMP tholeiites (e.g., Alibert, 1985; Bertrand, 1991; Bertrand et al., 1982; Cebriá et al., 2003; De Min et al., 2003; Deckart et al., 2005; Dostal & Durning, 1998; Dupuy et al., 1988; Heatherington & Mueller, 1999; Jourdan et al., 2003; Marsh, 1987; Merle et al., 2011; Pegrarn, 1990; Puffer, 1992; Puffer, 2003), including high-TiO₂ CAMP magmas from Sierra Leone (Callegaro et al., 2017). In Sierra Leone, high-TiO₂ gabbros of the Freetown Layered Complex exhibit an enriched isotopic signature characterized by very high ²⁰⁷Pb/²⁰⁴Pb_{201Ma} ratios but low ²⁰⁶Pb/²⁰⁴Pb_{201Ma} (Figure 2). A small amount of lamproite magma, inferred to derive from a local, subduction-metasomatized SCLM source, was tested as a plausible contributor, mixed with a dominant asthenospheric melt (Callegaro et al., 2017). A group of high-TiO₂ samples from South America (Merle et al., 2011) with comparatively low ²⁰⁷Pb/²⁰⁶Pb (Figure 2) may also sample a distinct, localized mantle or SCLM source (Merle et al., 2011). While a portion of the field for southern ENA CAMP Pb isotope signatures overlaps with that of Sierra Leone gabbros (Figure 2), they are otherwise distinct, having low TiO₂ contents, higher ⁸⁷Sr/⁸⁶Sr_{201Ma}, and lower ¹⁴³Nd/¹⁴⁴Nd_{201Ma} than the Freetown gabbros.

Without local volcanic samples inferred to derive from SCLM melt sources, or SCLM-derived local xenoliths for comparison, there are no regional Hf isotopic constraints for southern ENA SCLM, making it difficult to directly test for SCLM melt contributions to southern ENA

CAMP basalts. Eastern North American CAMP was located farther from cratonic or pericratonic settings than magmas from Brazil or Sierra Leone, though, suggesting SCLM is a less likely melt source for ENA. We further note that although there are rare exceptions (e.g., Griffin et al., 2000), global SCLM xenolith data largely have $\epsilon_{\text{Hf}} > +9$ (Choi et al., 2008, 2010; Shaw et al., 2007; Wittig et al., 2007, 2010) (Figure S2), making it difficult to explain the observed array primarily by this mechanism. We cannot completely rule out an exotic, metasomatized lithospheric mantle melt component influencing the composition of individual samples with slightly elevated ϵ_{Hf} (Figure 2a), but based on prior work, we consider it an unlikely overall melt source for low-TiO₂ LIP tholeiites.

4.2.3. Hypothesis 3: Paleozoic crustal recycling in the asthenosphere beneath CAMP

In a third scenario, we explore Paleozoic recycling of crustal material and production of a modified mantle source beneath ENA, which is subsequently melted during the CAMP event. Callegaro et al. (2013) suggested that ENA magmas may derive from direct melting of local asthenosphere containing 1) depleted upper mantle, 2) recycled upper continental crustal rocks, possibly as subducted Paleozoic terrigenous sediments associated with the assembly of Pangea, and 3) lower continental crustal rocks, perhaps delaminated and locally reintroduced into the convecting melt region (see e.g., Magni and Király, 2019). Whalen et al. (2015) suggested a related scenario in which melts and/or aqueous fluids derived from subducted sediments modified the local mantle melt source beneath ENA, with a stronger fluid-derived signature in the south and more melt metasomatism recorded to the north. Below, we explore the constraints that Hf isotopes would place on both models, and attempt to evaluate the possible role of Paleozoic recycled crust in ENA CAMP magma generation.

4.2.3.1. Paleozoic recycling of upper and lower continental crust.

Crustal recycling provides possible explanations for an incompatible-element enriched source with notably high Lu/Hf

ratios, as implied by the radiogenic $\epsilon_{\text{Hf}}^{201\text{Ma}}$ relative to $\epsilon_{\text{Nd}}^{201\text{Ma}}$ observed in southern ENA CAMP. As an initial test of melting a subduction-modified mantle source, we first consider whether direct mixing of local depleted asthenospheric mantle melts with recycled upper and local crust, i.e. the scenario suggested by Callegaro et al. (2013), can directly produce the observed data array (Figure 6). As discussed above, most continental crustal rocks plot along the terrestrial array, making it difficult to reproduce the southern ENA data trend. However, some lower crustal mafic granulites may inherit a high, decoupled ϵ_{Hf} ratio due to the presence of significantly old garnet with high Lu/Hf ratios (e.g., Blichert-Toft et al., 2005), similar to some of the xenoliths measured by Zartman et al. (2013). If recycled, e.g., by delamination into the asthenosphere, mafic LCC thus represents a plausible mantle source with elevated ϵ_{Hf} above the mantle array in Figure 2a. However, an additional unradiogenic (enriched) Hf source lying closer to the mantle array would then also be required to fully explain the observed ENA data. Upper continental crust is typically more enriched in incompatible elements and should plot along the mantle array (Table S1, Figures 2a, 4), making it a reasonable, additional recycled source and possibly lending support to the suggested model of Callegaro et al. (2013). Upper crustal material could have been introduced to the regional mantle by subduction of terrigenous marine sediments; if local sediment deposition occurred near a subducting margin and was relatively close to a weathering continental source, such sediments would closely resemble the average composition of nearby continental terranes, as modeled by Callegaro et al. (2013).

However, we observe that direct mixing of melts from ambient asthenosphere with a typical DM isotopic composition (Salters and Stracke, 2004; Workman and Hart, 2005) with recycled LCC and UCC material is unable to explain the Hf and Pb isotopes measured for southern ENA CAMP, at least within currently available constraints (e.g., Figure 2b). This is illustrated by the isotopic compositions of the suggested end-members in Table S1 and Figure 2b, where we identify a Proterozoic lower crustal end-member represented by mafic granulite Michigan

xenoliths (“Mafic LCC,” Zartman et al., 2013), an upper crust end-member represented by local average Carolina terrane (“UCC”) ($^{206}\text{Pb}/^{204}\text{Pb}$ ranges between ca. 17.1 and 17.5 for Carolina terrane rocks; Pettingill et al., 1984; Sinha et al., 1996), and ambient mantle modeled as a DM component (“DMM”). In particular, crustal components with ϵ_{Hf} and ϵ_{Nd} values capable of explaining the CAMP array do not span a sufficiently large range in Pb isotopic compositions to explain the measured data (Figure 2).

4.2.3.2. Paleozoic recycling and metasomatism of the asthenosphere. Alternatively, Whalen et al. (2015) suggested a scenario for the recycling of regional Paleozoic upper crustal sediments into the subcontinental asthenosphere without invoking lower crustal delamination. By incorporating subducted pelagic marine sediments, this scenario offers an alternative to recycled local UCC from the Carolina terrane, one that notably plots above the mantle array; such a component may thus alleviate the need for melting of exotic (i.e., with decoupled ϵ_{Hf} and ϵ_{Nd}) mafic Proterozoic LCC rocks. Unlike our upper crust estimate for the Carolina terrane, weathered terrigenous marine sediments have elevated Lu/Hf ratios due to the progressive removal of heavy detritus minerals like zircon during continental weathering and differential river transport; the elevated Lu/Hf ultimately produces high ϵ_{Hf} relative to ϵ_{Nd} in clay-rich marine pelagic sediments (Chauvel et al., 2014; Garcon et al., 2013, 2014; Vervoort et al., 1999, 2011). Chauvel et al. (2008) determined time-averaged ϵ_{Hf} and ϵ_{Nd} isotope compositions for typical subducted sediments, which reside in the same part of the Hf-Nd isotope diagram as both marine Fe-Mn precipitates and seawater (e.g., Albarede et al., 1998) (Figure 2a). As an alternative to the prior mixing scenario with upper and lower continental crust, here we test mixing of partial melts of depleted asthenosphere with a combination of 1) local Carolina terrane crust and 2) global average marine sediments (GLOSS, after Plank and Langmuir (1998) and Chauvel et al. (2008); Table S1). Specifically, we tested a Paleozoic marine sediment source subducted beneath the CAMP province during the construction of Pangea at

~370 Ma, i.e., 170 Ma prior to the CAMP melting event, after Merle et al. (2014), Callegaro et al. (2013), and Whalen et al. (2015).

In Figure 6a, where mixing results are reported along with our data, ternary mixing of depleted mantle, Carolina UCC crust, and average global sediment cannot account for the Hf-Nd isotopic variability observed in ENA samples. While trace element concentrations in recycled sources are necessarily averages of heterogeneous materials, and a small change in the trace element budget of upper crust, for example, may appear to resolve the observed discrepancy in mixing trajectories, the end members are inconsistent between diagrams. That is, average global subducted sediment has elevated ϵ_{Hf} relative to ϵ_{Nd} , similar to the southern ENA data array (e.g., Chauvel et al., 2008; Chen et al., 2013; Vervoort et al., 2011), but its highly radiogenic Pb isotope ratios are inconsistent with our most extreme samples, which have the lowest $\epsilon_{\text{Nd } 201\text{Ma}}$ but also the least radiogenic $^{206}\text{Pb}/^{204}\text{Pb}_{201\text{Ma}}$ and $^{207}\text{Pb}/^{204}\text{Pb}_{201\text{Ma}}$. While contributions of melts from recycled crustal rocks could thus explain some of the intermediate compositions observed in the ENA CAMP data set, the scenario is a poor explanation for the most unradiogenic samples with respect to $\epsilon_{\text{Hf } 201\text{Ma}}$.

A more plausible recycling hypothesis is the creation of a hybrid, metasomatised mantle source by the addition of subduction-derived fluids to the peridotitic mantle wedge, which in turn partially melts to produce local CAMP tholeiites. Whalen et al. (2015) suggested that the subducted sediments in the subcontinental CAMP asthenosphere have dehydrated and/or melted, producing fluids that metasomatically modified ambient peridotite. They further tied the nature of the metasomatic fluid (aqueous fluid in the south vs. silicate melt in the north) to geographic variations along the ENA subprovince as noted above.

Hafnium is primarily considered a tracer of melt and not aqueous fluid metasomatism in modern arc environments (e.g., Kempton et al., 2018), because Hf is expected to have relatively

low aqueous solubility (e.g., Banks, 1950; Linnen, 1998). However, the relatively low fluid mobility of Hf means dehydration of subducted sediments may produce a relatively high Lu/Hf metasomatic fluid, such that a modified mantle may develop relatively high ϵ_{Hf} ratios over time (e.g., Janney et al., 2005; Kempton et al., 2018). If northern ENA tholeiites record primarily melt metasomatism while southern ENA tholeiites record ancient fluid metasomatism of the regional mantle source, as posited by Whalen et al. (2015), southern ENA mantle could then have developed variably high ϵ_{Hf} compared to ϵ_{Nd} , while northern ENA mantle did not, similar to our observations; however, such a difference in fluid vs. melt metasomatic effects could be confounded by other factors. For instance, subducted metasediments may include stable metamorphic garnet, which could impact the Lu/Hf ratio of metasomatizing melts or fluids derived from the subducted rocks (e.g., Kempton et al., 2018). Some lithospheric mantle xenoliths that have experienced metasomatism also have extremely high ϵ_{Hf} ratios, unlike ENA CAMP basalts (e.g., Armytage et al., 2015). The impact of metasomatic source effects on long-term $^{176}\text{Hf}/^{177}\text{Hf}$ ratios is thus unclear and warrants more careful analysis.

Here we introduce a new model for calculating the trace element and isotope compositions of both subduction-modified depleted mantle wedge and subsequent partial melts of that modified mantle source (Table S4). In the model, three initial reservoirs are age-corrected to the time of subduction recycling: 1) ambient peridotite asthenosphere after Salters and Stracke's (2004) Depleted Mantle; 2) average global oceanic sediment similar to GLOSS (Chauvel et al., 2008; Plank and Langmuir, 1998); and 3) altered oceanic crust (AOC) calculated from Atlantic drill core compositions (Staudigel et al., 1996). The composition of a metasomatizing fluid is then determined for a range of mixtures of 1) an AOC-derived aqueous fluid and 2) either a melt or an aqueous fluid derived from subducted sediment. Trace element concentrations in all AOC and sediment-derived fluids are calculated using mobility and partition coefficients after Kogiso et al. (1997), Stracke et al. (2003), and Johnson and Plank (2000) (Table S3; see

Supporting Information). The composition of the modified wedge is then determined for 0-10% fluid addition to the mantle, and across the full range of fluid mixtures. Next, the resulting modified mantle composition is tracked for isotopic decay from the time of recycling and metasomatism (370 Ma) until the time of melting (201 Ma) to determine the isotopic and trace element compositions of the mantle during CAMP. Predicted trace element compositions in CAMP basalts were determined using a simple modal batch melting model and melt fraction of 6%, with garnet lherzolite mineral/melt partition coefficients and residual peridotite modes as in Table S3.

Results from the wedge metasomatism and melting model, shown in Figure 7, approach or overlap with the most isotopically depleted southern ENA CAMP basalt composition (sample CS49), as long as the subduction and recycling age is relatively young. The results shown in Figure 7 assume a Paleozoic subduction age of 370 Ma, i.e. the recycling age previously suggested by Merle et al. (2014), Callegaro et al. (2013), and Whalen et al. (2015). Recycling ages older than Paleozoic subduction fail to reproduce the $\epsilon_{\text{Hf}}^{201\text{Ma}}$, $\epsilon_{\text{Nd}}^{201\text{Ma}}$, and Pb isotope ratios observed in our basalts. Melting of a mantle source modified by a purely aqueous metasomatic fluid and dominated by sediment-derived fluid (i.e., the AOC-derived fluid $\leq 25\%$ of the fluid mixture) can reasonably explain sample CS49 with less than 10% fluid addition, although we note that the Pb isotope results shown in Figure 7c are close but not an exact fit to the measured data at the lowest fluid addition values ($< 4\%$) that work best for ϵ_{Hf} and ϵ_{Nd} isotopes.

We further note that for the most radiogenic Pb isotopes observed in ENA CAMP tholeiites, mantle metasomatism dominated by aqueous fluid addition is a closer match than melt metasomatism, even for some Newark basin samples (Figure 7c). This observation conflicts with the suggestion of Whalen et al. (2015) that differences in Paleozoic subduction angles

modified the metasomatic regime from north to south beneath the North American margin, and that more northerly ENA tholeiites were dominated by melt- and not aqueous fluid metasomatism of the Paleozoic mantle. We would argue that while the exact proportions of fluid addition to the mantle wedge may have been variable, a fluid-dominated metasomatic agent where most of the fluid is derived from subducted sediments (i.e., only a limited proportion of the fluid is contributed by AOC) provides a particularly good match to the radiogenic $^{206}\text{Pb}/^{204}\text{Pb}$ ENA end-member (Figure 7).

4.2.3.3. A hybrid recycling, metasomatism, and assimilation model for ENA CAMP.

While the most primitive ENA CAMP magma analyzed here is in good agreement with predictions for melting of metasomatized mantle, the remainder of our observed data array cannot be explained purely by melting of such a source, even if the nature of that metasomatism is itself regionally variable. Additional melting, mixing, and/or assimilation is thus required to explain the full isotopic range exhibited by southern ENA CAMP. As explored above, the compositions of southern ENA samples with low $\epsilon_{\text{Nd } 201\text{Ma}}$, comparatively radiogenic $\epsilon_{\text{Hf } 201\text{Ma}}$, and relatively low $^{206}\text{Pb}/^{204}\text{Pb}_{201\text{Ma}}$ cannot be easily explained by melt mixing. Of the possible sources considered here, only lower crustal granulites with decoupled Lu/Hf and Sm/Nd have the necessary isotopic signatures to plausibly explain this composition, but the required proportional contributions of melts from such a source are inconsistent in our calculations (Figure 8), and are too large for some of the resulting mixtures to be basaltic in major element composition. Based on the analysis above, we thus suggest that the ENA CAMP mantle melt source is dominated by fluid-metasomatized asthenosphere, perhaps containing moderate quantities of recycled continental crustal material, but not so much all of the observed data can be explained by direct melting of those recycled rocks. Some minor (generally < 10%) assimilation of zircon-bearing, intermediate-SiO₂, granulitic lower crust can then help to

explain much of the southern ENA data array (Figure 3). Our favored model thus includes a combination of factors, where some direct melting of recycled crust is plausible, but minor crustal assimilation is also favored, particularly to explain the southern ENA CAMP samples with the lowest $\epsilon_{\text{Hf } 201\text{Ma}}$ values. We consider this a plausible model to explain the systematic trend towards low $\epsilon_{\text{Nd } 201\text{Ma}}$ and $^{206}\text{Pb}/^{204}\text{Pb}_{201\text{Ma}}$ with comparatively high $\epsilon_{\text{Hf } 201\text{Ma}}$ and $^{207}\text{Pb}/^{204}\text{Pb}_{201\text{Ma}}$ in southern ENA basalts.

4.3. Broader petrogenesis of Central Atlantic Magmatic Province tholeiites

Figure 2a includes $^{176}\text{Hf}/^{177}\text{Hf}_{201\text{Ma}}$ results for magmas collected from other regions of CAMP, including Sierra Leone and Morocco (Table 2). The range of isotopic compositions across CAMP reflects localized processes, which for ENA include a local metasomatized mantle source and minor assimilation of local crustal rocks. Such localized variations extend to other parts of CAMP as well: samples from Sierra Leone, as noted above, exhibit notably high $\epsilon_{\text{Hf } 201\text{Ma}}$ values for a given $^{206}\text{Pb}/^{204}\text{Pb}_{201\text{Ma}}$ ratio (Figure 2b) and have been suggested to incorporate melts from local SCLM sources unique to that region, with an enriched composition comparable to worldwide anorogenic lamproites, e.g. from Western Australia, Gaussberg, or Leucite Hills (Callegaro et al., 2017). Likewise, in Pb isotope space, most magmas from CAMP form an array with high $^{207}\text{Pb}/^{204}\text{Pb}_{201\text{Ma}}$ for a given $^{206}\text{Pb}/^{204}\text{Pb}_{201\text{Ma}}$, while high-TiO₂ samples from South America have comparatively lower $^{207}\text{Pb}/^{204}\text{Pb}_{201\text{Ma}}$ for a given $^{206}\text{Pb}/^{204}\text{Pb}_{201\text{Ma}}$ (Figure 2) (Merle et al., 2011) and may instead sample a localized mantle or SCLM source, as noted above (Deckart et al., 2005; Merle et al., 2011). Central Atlantic Magmatic Province rocks from Guyana, Brazil, and Sierra Leone also include high-TiO₂ tholeiites (TiO₂ > 2 wt. %). The high-TiO₂ CAMP magma type, which exhibits very distinct isotopic signatures and trace element compositions (Marzoli et al., 2018), is volumetrically minor and confined to a narrow belt bordering the Western African Craton and the Amazonia

Craton/Guyana Shield (De Min et al., 2003; Deckart et al., 2005; Dupuy et al., 1988; Mauche et al., 1989).

The above observations indicate that a number of isotopic patterns are unique to specific regions within CAMP and sample localized sources in the underlying mantle. The more geographically restricted patterns do not clearly indicate a radially distributed hotspot-like signature that might directly support mantle plume influence. Even if the arrival of a plume head was associated with more widespread geographic dispersal and magma emplacement across broader terranes (e.g., McHone, 1996), making geographic emplacement patterns far from radial, such episodes should follow a sequence where first SCLM is melted due to thermal erosion, and then upwelling asthenospheric mantle melts (e.g., Ernst & Buchan, 2003; Ernst et al., 2001; Morgan, 1983). Based on isotope measurements and age information, neither scenario (geographically radial distribution of isotopic enrichment, or timing sequences indicative of large-scale lithospheric erosion and melting followed by asthenospheric melting) appears clear for CAMP.

Instead, the more localized geographic patterns appear to support regional upwelling and melting of local mantle, including localized melting of SCLM for some areas. Our observations could thus plausibly be explained either 1) by a regional passive upwelling response to lithospheric thinning, i.e., localized mantle convection response to rift initiation, or 2) by the arrival of a deep upwelling mantle plume and accompanying melting of entrained local asthenosphere and, in some areas, overlying lithosphere. A province-wide geochemical plume signature for CAMP thus remains ambiguous.

5. CONCLUSIONS

Eastern North American CAMP basalts were plausibly generated by melting of regionally upwelling, depleted upper mantle asthenosphere, which was likely metasomatized by aqueous

fluids derived from subducted oceanic crust and marine sediments. That melting may have been accompanied by direct melting of relatively minor quantities of previously recycled (e.g., subducted or delaminated) crustal rocks. Melting was likely then followed by assimilation of lower continental crust, possibly intermediate-SiO₂ granulites containing minor accessory minerals like zircon, which may influence the hafnium isotopic compositions of the basalts. The isotopic compositions of CAMP basalts do not directly support dominantly OIB-like, long-lived, enriched mantle source reservoir origins, but instead vary with local upper mantle and lithospheric compositions across the province, recording broad, regional mantle upwelling. Our findings thus suggest that continental rifting and the generation and emplacement of the CAMP flood basalt province are best explained by regional asthenospheric decompression beneath the Pangea supercontinent, neither requiring nor definitively precluding the influence of a deep-seated mantle plume on continental rifting.

Acknowledgments

We thank Jörg Geldmacher, Pamela Kempton, and two anonymous reviewers for providing thoughtful suggestions that helped improve a prior version of this manuscript. We also thank John Lassiter and Steve Shirey for productive discussions about CAMP. Daren Blythe and Nathan Sorsen assisted with sample preparation at UNL. L. Elkins acknowledges support from a UNL College of Arts and Sciences International Collaboration Award that funded this research. Field sampling was supported by the following grants: CARIPARO (Eccellenza 2008), PRIN (PRIN 20158A9CBM), Padova University (CPDA132295/13) to A. M. N. Youbi (Caddi Ayyad University, Marrakech, Morocco), H. Bertrand (ENS-Lyon, France), G. Bellieni (Padova University, Italy), S. Howard (South Carolina Survey), and M. Higgins (North Carolina Survey) are kindly thanked for help during fieldwork. Supporting data files are available at the IEDA data repository (<https://doi.org/10.1594/IEDA/111347>).

REFERENCES

Albarede, F., A. Simonetti, J. D. Vervoort, J. Blichert - Toft, and W. Abouchami (1998), A Hf - Nd isotopic correlation in ferromanganese nodules, *Geophysical Research Letters*, 25(20), 3895-3898.

Alibert, C. (1985), A Sr-Nd isotope and REE study of late Triassic dolerites from the Pyrenees (France) and the Messejana Dyke (Spain and Portugal), *Earth and Planetary Science Letters*, 73(1), 81-90.

Anderson, D. L. (1994), The sublithospheric mantle as the source of continental flood basalts: The case against the continental lithosphere and plume head reservoirs, *Earth and Planetary Science Letters*, 123, 269-280.

Armytage, R. M., A. D. Brandon, R. Andreasen, and T. J. Lapen (2015), Evolution of Mojavian mantle lithosphere influenced by Farallon plate subduction: Evidence from Hf and Nd isotopes in peridotite xenoliths from Dish Hill, CA, *Geochimica et Cosmochimica Acta*, 159, 264-284.

Baksi, A. K. (2003), Critical evaluation of $^{40}\text{Ar}/^{39}\text{Ar}$ ages for the Central Atlantic Magmatic Province: timing, duration and possible migration of magmatic centers, *Geophysical Monograph Series*, 136, 77-90.

Banks, H. O. (1950), The determination of the solubility of hafnium oxide in aqueous solution by the radioactive tracer technique, 4822 pp, School of Mines and Metallurgy of the University of Missouri, Rolla, Missouri.

Bédard, J. (1992), Jurassic quartz-normative tholeiite dikes from Anticosti Island, Quebec, In *Eastern North American Mesozoic Magmatism*, Eds. Puffer, J.H. and P.C. Ragland, *Special Papers-Geological Society of America*, v. 268, 161.

Begemann, F., K. Ludwig, G. Lugmair, K. Min, L. Nyquist, P. Patchett, P. Renne, C.-Y. Shih, I. M. Villa, and R. Walker (2001), Call for an improved set of decay constants for geochronological use, *Geochimica et Cosmochimica Acta*, 65(1), 111-121.

Béguelin, P., M. Bizimis, C. Beier, and S. Turner (2017), Rift–plume interaction reveals multiple generations of recycled oceanic crust in Azores lavas, *Geochimica et Cosmochimica Acta*, 218, 132-152.

Bertrand, H. (1991), *The Mesozoic tholeiitic province of Northwest Africa; a volcanotectonic record of the early opening of Central Atlantic*, In *Magmatism in extensional structural settings: the Phanerozoic African Plate*, Eds. Kampunzu, A.B. and R.T. Lubala, Springer-Verlag, Berlin, Germany.

Bertrand, H., J. Dostal, and C. Dupuy (1982), Geochemistry of early Mesozoic tholeiites from Morocco, *Earth and Planetary Science Letters*, 58(2), 225-239.

Bindeman, I. N., and O. E. Melnik (2016), Zircon survival, rebirth and recycling during crustal melting, magma crystallization, and mixing based on numerical modelling, *Journal of Petrology*, 57(3), 437-460.

Blackburn, T. J., P. E. Olsen, S. A. Bowring, N. M. McLean, D. V. Kent, J. Puffer, G. McHone, E. T. Rasbury, and M. Et-Touhami (2013), Zircon U-Pb geochronology links the end-Triassic extinction with the Central Atlantic Magmatic Province, *Science*, 340(6135), 941-945.

Blichert-Toft, J. (2001), On the Lu-Hf isotope geochemistry of silicate rocks, *Geostandards Newsletter-the Journal of Geostandards and Geoanalysis*, 25(1), 41-56.

Blichert-Toft, J., F. A. Frey, and F. Albarede (1999), Hf isotope evidence for pelagic sediments in the source of Hawaiian basalts, *Science*, 285(5429), 879-882.

Blichert-Toft, J., A. Agranier, M. Andres, R. Kingsley, J. G. Schilling, and F. Albarede (2005), Geochemical segmentation of the Mid-Atlantic Ridge north of Iceland and ridge-hot spot interaction in the North Atlantic, *Geochemistry Geophysics Geosystems*, 6, 10.1029/2004GC000788.

Bohrson, W. A., and F. J. Spera (2001), Energy-constrained open-system magmatic processes II: application of energy-constrained assimilation–fractional crystallization (EC-AFC) model to magmatic systems, *Journal of Petrology*, 42(5), 1019-1041.

Bouvier, A., J. D. Vervoort, and P. J. Patchett (2008), The Lu–Hf and Sm–Nd isotopic composition of CHUR: constraints from unequilibrated chondrites and implications for the bulk composition of terrestrial planets, *Earth and Planetary Science Letters*, 273(1-2), 48-57.

Bryan, S. E., and R. E. Ernst (2008), Revised definition of large igneous provinces (LIPs), *Earth-Science Reviews*, 86(1-4), 175-202.

Burov, E., and T. Gerya (2014), Asymmetric three-dimensional topography over mantle plumes, *Nature*, 513(7516), 85.

Callegaro, S., A. Marzoli, H. Bertrand, M. Chiaradia, L. Reisberg, C. Meyzen, G. Bellieni, R. E. Weems, and R. Merle (2013), Upper and lower crust recycling in the source of CAMP basaltic dykes from southeastern North America, *Earth and Planetary Science Letters*, 376, 186-199.

Callegaro, S., D.R. Baker, A. De Min, A. Marzoli, K. Geraki, H. Bertrand, C. Viti, and F. Nestola (2014), Enriched mantle source for the Central Atlantic magmatic province: New supporting evidence from southwestern Europe, *Lithos*, 188, 15-32.

Callegaro, S., A. Marzoli, H. Bertrand, J. Blichert-Toft, L. Reisberg, G. Cavazzini, F. Jourdan, J.H. Davies, L. Parisio, R. Bouchet, A. Paul, U. Schaltegger, M. Chiaradia (2017), Geochemical Constraints Provided by the Freetown Layered Complex (Sierra Leone) on the Origin of High-Ti Tholeiitic CAMP Magmas, *Journal of Petrology*, 58(9), 1811-1840.

Capriolo, M., A. Marzoli, L.E. Aradi, S. Callegaro, J. Dal Corso, R.J. Newton, B.J.W. Mills, P.B. Wignall, O. Bartoli, D.R. Baker, N. Youbi, L. Remusat, R. Spiess, and C. Szabó, (2020), Deep CO₂ in the end-Triassic Central Atlantic Magmatic Province, *Nature Communications* 11, 1670, doi: 10.1038/s41467-020-15325-6.

Carlson, R. (1991), Physical and chemical evidence on the cause and source characteristics of flood basalt volcanism, *Australian Journal of Earth Sciences*, 38(5), 525-544.

Cebriá, J. M., J. López-Ruiz, M. Doblas, L. T. Martins, and J. Munha (2003), Geochemistry of the Early Jurassic Messejana-Plasencia dyke (Portugal-Spain); Implications on the Origin of the Central Atlantic Magmatic Province, *Journal of Petrology*, 44, 547-568.

Chabou, M. C., H. Bertrand, and A. Sebaï (2010), Geochemistry of the Central Atlantic Magmatic Province (CAMP) in south-western Algeria, *Journal of African Earth Sciences*, 58, 211-219.

Chauvel, C., E. Lewin, M. Carpentier, N. T. Arndt, and J. C. Marini (2008), Role of recycled oceanic basalt and sediment in generating the Hf-Nd mantle array, *Nature Geoscience*, 1(1), 64-67.

Chauvel, C., E. Lewin, M. Carpentier, N. T. Arndt, and J.-C. Marini (2008), Role of recycled oceanic basalt and sediment in generating the Hf–Nd mantle array, *Nature geoscience*, 1(1), 64.

Chauvel, C., M. Garçon, S. Bureau, A. Besnault, B. M. Jahn, and Z. L. Ding (2014), Constraints from loess on the Hf-Nd isotopic composition of the upper continental crust, *Earth and Planetary Science Letters*, 388, 48-58.

Chen, T.-Y., G. Li, M. Frank, H.-F. Ling (2013), Hafnium isotope fractionation during continental weathering: Implications for the generation of the seawater Nd-Hf isotope relationships, *Geophysical Research Letters*, 40, 916-920.

Choi, S. H., S. B. Mukasa, X.-H. Zhou, X. H. Xian, and A. V. Andronikov (2008), Mantle dynamics beneath East Asia constrained by Sr, Nd, Pb and Hf isotopic systematics of ultramafic xenoliths and their host basalts from Hannuoba, North China, *Chemical Geology*, 248(1-2), 40-61.

Choi, S. H., K. Suzuki, S. B. Mukasa, J. I. Lee, and H. Jung (2010), Lu-Hf and Re-Os systematics of peridotite xenoliths from Spitsbergen, western Svalbard: Implications for mantle-crust coupling, *Earth and Planetary Science Letters*, 297(1-2), 121-132.

Cirilli, S., A. Marzoli, L. Tanner, H. Bertrand, N. Buratti, F. Jourdan, G. Bellieni, D. Kontak, and P. R. Renne (2009), Latest Triassic onset of the Central Atlantic Magmatic Province (CAMP) volcanism in the Fundy Basin (Nova Scotia): New stratigraphic constraints, *Earth and Planetary Science Letters*, 286, 514-525.

Coffin, M. F., and O. Eldholm (1992), Volcanism and continental break-up; a global compilation of large igneous provinces, *Geological Society Special Publications*, 68, 17-30.

Coltice, N., B. Phillips, H. Bertrand, Y. Ricard, and P. Rey (2007), Global warming of the mantle at the origin of flood basalts over supercontinents, *Geology*, 35(5), 391-394.

Courtillot, V., C. Jaupart, I. Manighetti, P. Tapponnier, and J. Besse (1999), On causal links between flood basalts and continental breakup, *Earth and Planetary Science Letters*, 166, 177-195.

Davies, J. H. F. L., A. Marzoli, H. Bertrand, N. Youbi, M. Ernesto, and U. Schaltegger (2017), End-Triassic mass extinction started by intrusive CAMP activity, *Nature Communications*, 8, 15596.

De Boer, J. (1992), Stress configurations during and following emplacement of ENA basalts in the northern Appalachians, In *Eastern North American Mesozoic Magmatism*, Eds. Puffer, J.H. and P.C. Ragland, *Special Papers-Geological Society of America*, 268, 361.

De Min, A., E. M. Piccirillo, A. Marzoli, G. Bellieni, P. R. Renne, M. Ernesto, and L. S. Marques (2003), The Central Atlantic Magmatic Province (CAMP) in Brazil: petrology, geochemistry, $^{40}\text{Ar}/^{39}\text{Ar}$ ages, paleomagnetism and geodynamic implications, *Geophysical Monograph Series*, 136, 91-128.

Deckart, K., G. Féraud, and H. Bertrand (1997), Age of Jurassic continental tholeiites of French Guyana, Surinam and Guinea: Implications for the initial opening of the Central Atlantic Ocean, *Earth and Planetary Science Letters*, 150, 205-220.

Deckart, K., H. Bertrand, and J.-P. Liégeois (2005), Geochemistry and Sr, Nd, Pb isotopic composition of the Central Atlantic Magmatic Province (CAMP) in Guyana and Guinea, *Lithos*, 82, 289-314.

Dorais, M. J., and M. Tubrett (2008), Identification of a subduction zone component in the Higganum dike, Central Atlantic Magmatic Province: A LA - ICPMS study of clinopyroxene with implications for flood basalt petrogenesis, *Geochemistry, Geophysics, Geosystems*, 9(10).

Dorais, M. J., M. Harper, S. Larson, H. Nugroho, P. Richardson, and N. Roosmawati (2005), A comparison of Eastern North America and Coastal New England magma suites: implications for subcontinental mantle evolution and the broad-terrane hypothesis, *Canadian Journal Earth Sci.*, *42*(1571-1587).

Dostal, J., and C. Dupuy (1984), Geochemistry of the North Mountain Basalts (Nova Scotia, Canada), *Chemical Geology*, *45*(3), 245-261.

Dostal, J., and M. Durning (1998), Geochemical constraints on the origin and evolution of early Mesozoic dikes in Atlantic Canada, *European Journal Mineralogy*, *10*, 79-93.

Dunning, G. R., and J. P. Hodych (1990), U/Pb zircon and baddeleyite ages for the Palisades and Gettysburg sills of the northeastern United States: Implications for the age of the Triassic/Jurassic boundary, *Geology*, *18*, 795-798.

Dupuy, C., J. Marsh, J. Dostal, A. Michard, and S. Testa (1988), Asthenospheric and lithospheric sources for Mesozoic dolerites from Liberia (Africa): trace element and isotopic evidence, *Earth and Planetary Science Letters*, *87*(1), 100-110.

Eisele, J., M. Sharma, S. J. Galer, J. Blichert-Toft, C. W. Devey, and A. W. Hofmann (2002), The role of sediment recycling in EM-1 inferred from Os, Pb, Hf, Nd, Sr isotope and trace element systematics of the Pitcairn hotspot, *Earth and Planetary Science Letters*, *196*(3), 197-212.

Ernst, R. E., and K. L. Buchan (2003), Recognizing Mantle Plumes in the Geological Record, *Annual Reviews Earth Planetary Science*, *31*, 469-523.

Ernst, R. E., E. B. Grosfils, and D. Mège (2001), Giant Dike Swarms: Earth, Venus, and Mars, *Annual Reviews Earth Planetary Science*, *29*, 489-534.

Falloon, T.J. and L.V. Danyushevsky (2000), Melting of refractory mantle at 1.5, 2 and 2.5 GPa under anhydrous and H₂O-undersaturated conditions: Implications for the petrogenesis of high-Ca boninites and the influence of subduction components on mantle melting, *Journal of Petrology*, 41(2), 257-283.

Frisby, C., M. Bizimis, and S. Mallick (2016), Hf-Nd isotope decoupling in bulk abyssal peridotites due to serpentinization, *Chemical Geology*, 440, 60-72.

Garcon, M., C. Chauvel, C. France-Lanord, P. Huyghe, and J. Lave (2013), Continental sedimentary processes decouple Nd and Hf isotopes, *Geochimica Et Cosmochimica Acta*, 121, 177-195.

Garcon, M., C. Chauvel, C. France-Lanord, M. Limonta, and E. Garzanti (2014), Which minerals control the Nd-Hf-Sr-Pb isotopic compositions of river sediments?, *Chemical Geology*, 364, 42-55.

Geldmacher, J., K. Hoernle, B. B. Hanan, J. Blichert-Toft, F. Hauff, J. B. Gill, and H.-U. Schmincke (2011), Hafnium isotopic variations in East Atlantic intraplate volcanism, *Contributions to Mineralogy and Petrology*, 162(1), 21-36.

Gillard, M., D. Sauter, J. Tugend, S. Tomasi, M.-E. Epin, and G. Manatschal (2017), Birth of an oceanic spreading center at a magma-poor rift system, *Scientific reports*, 7(1), 15072.

Griffin, W., N. Pearson, E. Belousova, S. v. Jackson, E. Van Achtebergh, S. Y. O'Reilly, and S. Shee (2000), The Hf isotope composition of cratonic mantle: LAM-MC-ICPMS analysis of zircon megacrysts in kimberlites, *Geochimica et Cosmochimica Acta*, 64(1), 133-147.

Guo, W., S. Zhao, F. Wang, Z. Yang, S. Jia, and Z. Liu (2019), Crustal structure of the eastern Piedmont and Atlantic coastal plain in North Carolina and Virginia, eastern North American margin, *Earth, Planets and Space*, 71(1), 69.

Halliday, A. N., A. P. Dickin, R. N. Hunter, G. R. Davies, T. J. Dempster, P. J. Hamilton, and B. G. Upton (1993), Formation and composition of the lower continental crust: evidence from Scottish xenolith suites, *Journal of Geophysical Research: Solid Earth*, 98(B1), 581-607.

Hames, W. E., P. R. Renne, and C. Ruppel (2000), New evidence for geologically instantaneous emplacement of earliest Jurassic Central Atlantic magmatic province basalts on the North American margin, *Geology*, 28, 859-862.

Heatherington, A. L., and P. A. Mueller (1999), Lithospheric sources of North Florida, USA tholeiites and implications for the origin of the Suwannee terrane, *Lithos*, 46, 215-233.

Heimdal, T. H., H. H. Svensen, J. Ramezani, K. Iyer, E. Pereira, R. Rodrigues, M. T. Jones, and S. Callegaro (2018), Large-scale sill emplacement in Brazil as a trigger for the end-Triassic crisis, *Scientific Reports*, 8, 141.

Heinonen, A., I. Mänttari, O.T. Rämö, T. Andersen, and K. Larjamo (2016), A prior evidence for zircon antecryst entrainment in megacrystic Proterozoic granites, *Geology*, 44, 227-230.

Hermes, O. (1964), A quantitative petrographic study of dolerite in the Deep River Basin, North Carolina, *Am. Mineral*, 49, 1718-1729.

Herzberg, C., and E. Gazel (2009), Petrological evidence for secular cooling in mantle plumes, *Nature*, 458(7238), 619.

Hesselbo, S. P., S. A. Robinson, F. Surlyk, and S. Piasecki (2002), Terrestrial and marine extinction at the Triassic-Jurassic boundary synchronized with major carbon-cycle perturbation: A link to initiation of massive volcanism?, *Geology*, 30(3), 251-254.

Hill, R. I. (1991), Starting plumes and continental break-up, *Earth and Planetary Science Letters*, 104(2), 398-416.

Hodych, J. P., and G. R. Dunning (1992), Did the Manicouagan impact trigger end-of-Triassic mass extinction?, *Geology*, 20, 51-54.

Holbrook, W., and P. Kelemen (1993), Large igneous province on the US Atlantic margin and implications for magmatism during continental breakup, *Nature*, 364(6436), 433-436.

Holbrook, W. S., E. Reiter, G. Purdy, D. Sawyer, P. Stoffa, J. Austin Jr, J. Oh, and J. Makris (1994), Deep structure of the US Atlantic continental margin, offshore South Carolina, from coincident ocean bottom and multichannel seismic data, *Journal of Geophysical Research*, 99(B5), 9155-9178.

Hole, M. J. (2015), The generation of continental flood basalts by decompression melting of internally heated mantle, *Geology*, 43(4), 311-314.

Holm, P.M., J.R. Wilson, B.P. Christensen, L. Hansen, S.L. Hansen, K.M. Hein, A.K. Mortensen, R. Pedersen, S. Plesner, and M.K. Runge (2006), Sampling the Cape Verde Mantle Plume: Evolution of melt compositions on Santo Antão, Cape Verde Islands. *Journal of Petrology*, 47, 145-189.

Huang, Y.-M., P. Van Calsteren, and C. I. Hawkesworth (1995), The evolution of the lithosphere in southern Africa: a perspective on the basic granulite xenoliths from kimberlites in South Africa, *Geochimica et Cosmochimica Acta*, 59(23), 4905-4920.

Iacumin, M., A. De Min, E. M. Piccirillo, and G. Bellieni (2003), Source mantle heterogeneity and its role in the genesis of Late Archaean-Proterozoic (2.7-1.0 Ga) and Mesozoic (200 and 130 Ma) tholeiitic magmatism in the South American Platform, *Earth-Science Reviews*, 62, 365-397.

Ingle, S., P. A. Mueller, A. L. Heatherington, and M. Kozuch (2003), Isotopic evidence for the magmatic and tectonic histories of the Carolina terrane: implications for stratigraphy and terrane affiliation, *Tectonophysics*, 371(1-4), 187-211.

Jackson, M.G., S.R. Hart, A.P. Koppers, H. Staudigel, J. Konter, J. Blusztajn, M. Kurz, and J.A. Russell (2007), The return of subducted continental crust in Samoan lavas, *Nature*, 448, 684-687.

Jackson, M. G., and R. Dasgupta (2008), Compositions of HIMU, EM1, and EM2 from global trends between radiogenic isotopes and major elements in ocean island basalts, *Earth and Planetary Science Letters*, 276(1-2), 175-186.

Jaffey, A. H., K. F. Flynn, Glendeni.Le, W. C. Bentley, and A. M. Essling (1971), Precision Measurement of Half-Lives and Specific Activities of U-235 and U-238, *Physical Review C*, 4(5), 1889-1906.

Janney, P. E., and P. R. Castillo (2001), Geochemistry of the oldest Atlantic oceanic crust suggests mantle plume involvement in the early history of the central Atlantic Ocean, *Earth and Planetary Science Letters*, 192, 291-302.

Janney, P., A. Le Roex, and R. Carlson (2005), Hafnium isotope and trace element constraints on the nature of mantle heterogeneity beneath the central Southwest Indian Ridge (13 E to 47 E), *Journal of Petrology*, 46(12), 2427-2464.

Johnson, M. C., and T. Plank (2000), Dehydration and melting experiments constrain the fate of subducted sediments, *Geochemistry, Geophysics, Geosystems*, 1(12), doi: 10.1029/1999GC000014.

Jourdan, F., A. Marzoli, H. Bertrand, M. Cosca, and D. Fontignie (2003), The northernmost CAMP: $^{40}\text{Ar}/^{39}\text{Ar}$ age, petrology and Sr-Nd-Pb isotope geochemistry of the Kerforne dike, Brittany, France, *Geophysical Monograph Series*, 136, 209-226.

Jourdan, F., H. Bertrand, U. Schärer, J. Blichert-Toft, G. Féraud, and A. B. Kampunzu (2007), Major and trace element and Sr, Nd, Hf, and Pb isotope compositions of the Karoo Large Igneous Province, Botswana-Zimbabwe: Lithosphere vs mantle plume contribution, *Journal of Petrology*, 48(6), 1043-1077.

Jourdan, F., A. Marzoli, H. Bertrand, S. Cirilli, L. H. Tanner, D. J. Kontak, G. McHone, P. R. Renne, and G. Bellieni (2009), $^{40}\text{Ar}/^{39}\text{Ar}$ ages of CAMP in North America: Implications for the Triassic-Jurassic boundary and the ^{40}K decay constant bias, *Lithos*, 110, 167-180.

Kempton, P. D., H. Downes, and M. Lustrino (2018), Pb and Hf isotope evidence for mantle enrichment processes and melt interactions in the lower crust and lithospheric mantle in Miocene orogenic volcanic rocks from Monte Arcuentu (Sardinia, Italy), *Geosphere*, 14(3), 926-950.

Kent, R. (1991), Lithospheric uplift in eastern Gondwana: Evidence for a long-lived mantle plume system?, *Geology*, 19(1), 19-23.

Khanna, T., M. Bizimis, G. Yogodzinski, and S. Mallick (2014), Hafnium-neodymium isotope systematics of the 2.7 Ga Gadwal greenstone terrane, Eastern Dharwar craton, India: Implications for the evolution of the Archean depleted mantle, *Geochimica Et Cosmochimica Acta*, 127, 10-24.

Klein, E. M. (2004), Geochemistry of the Igneous Ocean Crust, in *Treatise on Geochemistry*, edited by H. D. Holland and K. K. Turekian, pp. 433-463, Elsevier, Amsterdam.

Klügel, A., K. Galipp, K. Hoernle, F. Hauff, and S. Groom (2017), Geochemical and volcanological evolution of La Palma, Canary Islands. *Journal of Petrology*, 58, 1227-1248.

Knight, K. B., S. Nomade, P. R. Renne, A. Marzoli, H. Bertrand, and N. Youbi (2004), The Central Atlantic Magmatic Province at the Triassic-Jurassic boundary: paleomagnetic and $^{40}\text{Ar}/^{39}\text{Ar}$ evidence from Morocco for brief, episodic volcanism, *Earth and Planetary Science Letters*, 228, 143-160.

Kogiso, T., Y. Tatsumi, and S. Nakano (1997), Trace element transport during dehydration processes in the subducted oceanic crust: 1. Experiments and implications for the origin of ocean island basalts, *Earth and Planetary Science Letters*, 148(1-2), 193-205.

Kontak, D. J. (2008), On the edge of CAMP: Geology and volcanology of the Jurassic North Mountain Basalt, Nova Scotia, *Lithos*, 101, 74-101.

Koptev, A., E. Calais, E. Burov, S. Leroy, and T. Gerya (2015), Dual continental rift systems generated by plume–lithosphere interaction, *Nature Geoscience*, 8(5), 388.

Linnen, R. L. (1998), The solubility of Nb-Ta-Zr-Hf-W in granitic melts with Li and Li + F; constraints for mineralization in rare metal granites and pegmatites, *Economic Geology*, 93, 1013-1025.

Lizarralde, D., and W. S. Holbrook (1997), US mid-Atlantic margin structure and early thermal evolution, *Journal of Geophysical Research*, 102, 22.

Magni, V. and A. Király (2019), Delamination, Reference Module in Earth Systems and Environmental Sciences, Elsevier.

Mallick, S., J. J. Standish, and M. Bizimis (2015), Constraints on the mantle mineralogy of an ultra-slow ridge: Hafnium isotopes in abyssal peridotites and basalts from the 9-25°E Southwest Indian Ridge, *Earth and Planetary Science Letters*, 410, 42-53.

Marsh, J. S. (1987), Basalt geochemistry and tectonic discrimination within continental flood basalt provinces, *Journal of Volcanology and Geothermal Research*, 32(1-3), 35-49.

Marzoli, A., P. R. Renne, E. M. Piccirillo, M. Ernesto, G. Bellieni, and A. De Min (1999), Extensive 200-Million-Year-Old Continental Flood Basalts of the Central Atlantic Magmatic Province, *Science*, 284, 616-618.

Marzoli, A., H. Bertrand, K.B. Knight, S. Cirilli, C. Verati, S. Nomade, P.R. Renne, N. Youbi, R. Martini, K. Allenbach, R. Neuwerth, C. Rapaille, L. Zaninetti, and G. Bellieni (2004), Synchrony of the Central Atlantic magmatic province and the Triassic-Jurassic boundary climatic and biotic crisis, *Geology*, 32, 973-976.

Marzoli, A., F. Jourdan, J. H. Puffer, T. Cuppone, L. H. Tanner, R. E. Weems, H. Bertrand, S. Cirilli, G. Bellieni, and A. De Min (2011), Timing and duration of the Central Atlantic magmatic province in the Newark and Culpeper basins, eastern U.S.A., *Lithos*, 122, 175-188.

Marzoli, A., F. Jourdan, F. Bussy, M. Chiaradia, and F. Costa (2014), Petrogenesis of tholeiitic basalts from the Central Atlantic magmatic province as revealed by mineral major and trace elements and Sr isotopes, *Lithos*, 188, 44-59.

Marzoli, A., S. Callegaro, J. Dal Corso, J. H. F. L. Davies, M. Chiaradia, N. Youbi, H. Bertrand, L. Reisberg, R. Merle, and F. Jourdan (2018), The Central Atlantic Magmatic Province (CAMP): A Review, in *The Late Triassic World: Earth in a Time of Transition*, edited by L. H. Tanner, pp. 91-125, Springer International Publishing, Cham.

Marzoli, A., H. Bertrand, N. Youbi, S. Callegaro, R. Merle, L. Reisberg, M. Chiaradia, S. Brownlee, F. Jourdan, and A. Zanetti (2019), The Central Atlantic magmatic province (CAMP) in Morocco, *Journal of Petrology*, 60, 945-996.

Mauche, R., G. Faure, L. M. Jones, and J. Hoefs (1989), Anomalous isotopic compositions of Sr, Ar and O in the Mesozoic diabase dikes of Liberia, West Africa, *Contributions to Mineralogy and Petrology*, 101(1), 12-18.

May, P. R. (1971), Pattern of Triassic-Jurassic Diabase Dikes around the North Atlantic in the Context of Predrift Position of the Continents, *Geological Society of America Bulletin*, 82, 1285-1292.

Mazza, S. E., E. Gazel, E. A. Johnson, M. Bizimis, R. McAleer, and C. B. Biryol (2017), Post - rift magmatic evolution of the eastern North American “passive - aggressive” margin, *Geochemistry, Geophysics, Geosystems*, 18(1), 3-22.

Mazza, S. E., E. Gazel, M. Bizimis, R. Moucha, P. Béguelin, E. A. Johnson, R. J. McAleer, and A. V. Sobolev (2019), Sampling the volatile-rich transition zone beneath Bermuda, *Nature*, 569(7756), 398.

McHone, J. G. (1978), Distribution, orientations, and ages of mafic dikes in central New England, *Geological Society of America Bulletin*, 89(11), 1645-1655.

McHone, G. (1996), Broad-terrane Jurassic flood basalts across northeastern North America, *Geology*, 24, 319-322.

McHone, J. G. (2000), Non-plume magmatism and rifting during the opening of the central Atlantic Ocean, *Tectonophysics*, 316, 287-296.

McKenzie, D., and R. O'Nions (1991), Partial Melt Distributions From Inversion Of Rare-Earth Element Concentrations, *Journal of Petrology*, 32, 1021.

Merle, R., A. Marzoli, H. Bertrand, L. Reisberg, C. Verati, C. Zimmermann, M. Chiaradia, and G. Bellieni (2011), $^{40}\text{Ar}/^{39}\text{Ar}$ ages and Sr-Nd-Pb-Os geochemistry of CAMP tholeiites from Western Maranhao basin (NE Brazil), *Lithos*, 122, 137-151.

Merle, R., A. Marzoli, L. Reisberg, H. Bertrand, A. Nemchin, M. Chiaradia, S. Callegaro, F. Jourdan, G. Bellieni, D. Kontak, J. Puffer, and J.G. McHone (2014), Sr, Nd, Pb and Os Isotope Systematics of CAMP Tholeiites from Eastern North America (ENA): Evidence of a Subduction-enriched Mantle Source, *Journal of Petrology*, 55(1), 133-180.

Morgan, P. (1983), Constraints on rift thermal processes from heat flow and uplift, *Tectonophysics*, 94(1), 277-298.

Münker, C., S. Weyer, E. Scherer, and K. Mezger (2001), Separation of high field strength elements (Nb, Ta, Zr, Hf) and Lu from rock samples for MC-ICPMS measurements, *Geochem. Geophys. Geosyst.*, 2(12), doi: 10.1029/2001GC000183.

Nehring, F., S.F. Foley, and P. Hölttä (2010), Trace element partitioning in the granulite facies, *Contrib. Mineral. Petrol.*, 159, 493-519.

Nomade, S., K. Knight, E. Beutel, P. Renne, C. Verati, G. Féraud, A. Marzoli, N. Youbi, and H. Bertrand (2007), Chronology of the Central Atlantic Magmatic Province: Implications for the Central Atlantic rifting processes and the Triassic-Jurassic biotic crisis, *Palaeogeography, Palaeoclimatology, Palaeoecology*, 244(1), 326-344.

Oyarzun, R., M. Doblas, J. López-Ruiz, and J. M. Cebriá (1997), Opening of the central Atlantic and asymmetric mantle upwelling phenomena: implications for long-lived magmatism in western North Africa and Europe, *Geology*, 25(8), 727-730.

Papezik, V., J. D. Greenough, J. A. Colwell, and T. J. Mallinson (1988), North Mountain basalt from Digby, Nova Scotia: models for a fissure eruption from stratigraphy and petrochemistry, *Canadian Journal of Earth Sciences*, 25(1), 74-83.

Pe-Piper, G., and D. J. W. Piper (1999), Were Jurassic tholeiitic lavas originally widespread in southeastern Canada?: a test of the broad terrane hypothesis, *Canadian Journal of Earth Sciences*, 36(9), 1509-1516.

Pegram, W. J. (1990), Development of continental lithospheric mantle as reflected in the chemistry of the Mesozoic Appalachian tholeiites, USA, *Earth and Planetary Science Letters*, 97(3), 316-331.

Pettingill, H. S., A. Sinha, and M. Tatsumoto (1984), Age and origin of anorthosites, charnockites, and granulites in the central Virginia Blue Ridge: Nd and Sr isotopic evidence, *Contributions to Mineralogy and Petrology*, 85(3), 279-291.

Plank, T., and C. H. Langmuir (1998), The chemical composition of subducting sediment and its consequences for the crust and mantle, *Chemical geology*, 145(3), 325-394.

Puffer, J. (1992), Eastern North American flood basalts in the context of the incipient breakup of Pangea, , In *Eastern North American Mesozoic Magmatism*, Eds. Puffer, J.H. and P.C. Ragland, *Special Papers-Geological Society of America*, v. 268, 95.

Puffer, J. (2001), Contrasting high field strength element contents of continental flood basalts from plume versus reactivated-arc sources, *Geology*, 29(8), 675-678.

Puffer, J. H. (2003), A reactivated back-arc source for CAMP magma, *Geophysical Monograph Series*, 136, 151-162.

Puffer, J., D. Hurtubise, F. Geiger, and P. Lechler (1981), Chemical composition and stratigraphic correlation of the Mesozoic basalt units of the Newark Basin, New Jersey, and the Hartford Basin, Connecticut, *Geological Society of America Bulletin*, 92, 515-553.

Ragland, P., L. Cummins, and J. Arthur (1992), Compositional patterns for early Mesozoic diabases from South Carolina to central Virginia, In *Eastern North American Mesozoic Magmatism*, Eds. Puffer, J.H. and P.C. Ragland, *Special Papers-Geological Society of America*, v. 268, 309.

Reinemund, J. A. (1955), *Geology of the Deep River coal field, North Carolina*, Geological Survey Professional Paper 246, U.S. Government Printing Office, Washington, D.C.

Rey, P. F. (2015), The geodynamics of mantle melting, *Geology*, 43(4), 367-368.

Ruiz-Martínez, V. C., T. H. Torsvik, D. J. J. van Hinsbergen, and C. Gaina (2012), Earth at 200Ma: Global palaeogeography refined from CAMP palaeomagnetic data, *Earth and Planetary Science Letters*, 331, 67-79.

Salters, V. J. M., and S. R. Hart (1989), The Hafnium Paradox and the Role of Garnet in the Source of Mid-Ocean-Ridge Basalts, *Nature*, 342(6248), 420-422.

Salters, V. J., and A. Stracke (2004), Composition of the depleted mantle, *Geochemistry, Geophysics, Geosystems*, 5(5), doi: 10.1029/2003GC000597.

Salters, V. J., J. Blichert-Toft, Z. Fekiacova, A. Sachi-Kocher, and M. Bizimis (2006), Isotope and trace element evidence for depleted lithosphere in the source of enriched Ko'olau basalts, *Contributions to Mineralogy and Petrology*, 151(3), 297-312.

Salters, V. J., S. Mallick, S. R. Hart, C. E. Langmuir, and A. Stracke (2011), Domains of depleted mantle: New evidence from hafnium and neodymium isotopes, *Geochemistry, Geophysics, Geosystems*, 12(8), doi: 10.1029/2011GC003617.

Saunders, A. D., S. M. Jones, L. A. Morgan, K. L. Pierce, M. Widdowson, and Y. G. Xu (2007), Regional uplift associated with continental large igneous provinces; the roles of mantle plumes and the lithosphere, *Chemical Geology*, 241(3-4), 282-318.

Schmitz, M. D., J. D. Vervoort, S. A. Bowring, and P. J. Patchett (2004), Decoupling of the Lu-Hf and Sm-Nd isotope systems during the evolution of granulitic lower crust beneath southern Africa, *Geology*, 32(5), 405-408.

Sebai, A., G. Feraud, H. Bertrand, and J. Hanes (1991), $^{40}\text{Ar}/^{39}\text{Ar}$ dating and geochemistry of tholeiitic magmatism related to the early opening of the Central Atlantic Rift, *Earth and Planetary Science Letters*, 104(2), 455-472.

Sengör, A., and K. Burke (1978), Relative timing of rifting and volcanism on Earth and its tectonic implications, *Geophysical Research Letters*, 5(6), 419-421.

Shaw, J., J. Baker, A. Kent, K. Ibrahim, and M. Menzies (2007), The geochemistry of the Arabian lithospheric mantle—a source for intraplate volcanism?, *Journal of Petrology*, 48(8), 1495-1512.

Shellnutt, J. G., J. Dostal, and M.-W. Yeh (2018), Mantle source heterogeneity of the Early Jurassic basalt of eastern North America, *International Journal of Earth Sciences*, 107(3), 1033-1058.

Sinha, A., J. Hogan, and J. Parks (1996), Lead Isotope Mapping of Crustal Reservoirs Within the Grenville Superterrene: I. Central and Southern Appalachians, *Geophysical Monograph-American Geophysical Union*, 95, 293-306.

Sobolev, S. V., A. V. Sobolev, D. V. Kuzmin, N. A. Krivolutskaya, A. G. Petrunin, N. T. Arndt, V. A. Radko, and Y. R. Vasiliev (2011), Linking mantle plumes, large igneous provinces and environmental catastrophes, *Nature*, 477(7364), 312-316.

Söderlund, U., P. J. Patchett, J. D. Vervoort, and C. E. Isachsen (2004), The ^{176}Lu decay constant determined by Lu–Hf and U–Pb isotope systematics of Precambrian mafic intrusions, *Earth and Planetary Science Letters*, 219(3-4), 311-324.

Spera, F. J., and W. A. Bohron (2001), Energy-constrained open-system magmatic processes I: General model and energy-constrained assimilation and fractional crystallization (EC-AFC) formulation, *Journal of Petrology*, 42(5), 999-1018.

Staudigel, H., T. Plank, B. White, and H. U. Schmincke (1996), Geochemical fluxes during seafloor alteration of the basaltic upper oceanic crust: DSDP Sites 417 and 418, *Subduction: top to bottom*, 96, 19-38.

Stracke, A., M. Bizimis, and V. J. M. Salters (2003), Recycling oceanic crust: Quantitative constraints, *Geochemistry, Geophysics, Geosystems*, 4(3), 8003.

Taylor, S. R., and S. M. McLennan (1995), The geochemical evolution of the continental crust, *Reviews of Geophysics*, 33(2), 241-265.

Tollo, R., and D. Gottfried (1992), Petrochemistry of Jurassic basalt from eight cores, Newark basin, New Jersey, In *Eastern North American Mesozoic Magmatism*, Eds. Puffer, J.H. and P.C. Ragland, *Special Papers-Geological Society of America*, v. 268, 233.

Verati, C., H. Bertrand, and G. Féraud (2005), The farthest record of the Central Atlantic Magmatic Province into West Africa craton: Precise $^{40}\text{Ar}/^{39}\text{Ar}$ dating and geochemistry of Taoudenni basin intrusives (northern Mali), *Earth and Planetary Science Letters*, 235(1), 391-407.

Verati, C., C. Rapaille, G. Féraud, A. Marzoli, H. Bertrand, and N. Youbi (2007), $^{40}\text{Ar}/^{39}\text{Ar}$ ages and duration of the Central Atlantic Magmatic Province volcanism in Morocco and Portugal and its relation to the Triassic-Jurassic boundary, *Palaeogeography, Palaeoclimatology, Palaeoecology*, 244(1), 308-325.

Vervoort, J. D., P. J. Patchett, J. Blichert-Toft, and F. Albarede (1999), Relationships between Lu-Hf and Sm-Nd isotopic systems in the global sedimentary system, *Earth and Planetary Science Letters*, 168(1-2), 79-99.

Vervoort, J. D., P. J. Patchett, F. Albarede, J. Blichert-Toft, R. Rudnick, and H. Downes (2000), Hf-Nd isotopic evolution of the lower crust, *Earth and Planetary Science Letters*, 181(1-2), 115-129.

Vervoort, J. D., T. Plank, and J. Prytulak (2011), The Hf-Nd isotopic composition of marine sediments, *Geochimica Et Cosmochimica Acta*, 75, 5903-5926.

Wedepohl, K. H. (1995), The composition of the continental crust, *Geochimica et cosmochimica Acta*, 59(7), 1217-1232.

Weigand, P. W., and P. C. Ragland (1970), Geochemistry of Mesozoic dolerite dikes from eastern North America, *Contributions to Mineralogy and Petrology*, 29(3), 195-214.

Whalen, L., E. Gazel, C. Vidito, J. Puffer, M. Bizimis, W. Henika, and M. J. Caddick (2015), Supercontinental inheritance and its influence on supercontinental breakup: The Central

Atlantic Magmatic Province and the breakup of Pangea, *Geochemistry Geophysics Geosystems*, 16(10), 3532-3554.

White, R. S., and D. P. McKenzie (1989), Volcanism at Rifts, *Scientific American*, 261(1), 62-71.

Willbold, M., and A. Stracke (2006), Trace element composition of mantle end-members: Implications for recycling of oceanic and upper and lower continental crust, *Geochem. Geophys. Geosyst.*, 7(4), doi: 10.1029/2005GC001005.

Wilson, J. T. (1966), Did the Atlantic close and then re-open?, *Nature*, 211, 676-681.

Wilson, M. (1997), Thermal evolution of the Central Atlantic passive margins: continental break-up above a Mesozoic super-plume, *Journal of the Geological Society*, 154(3), 491-495.

Wittig, N., J. A. Baker, and H. Downes (2007), U–Th–Pb and Lu–Hf isotopic constraints on the evolution of sub-continental lithospheric mantle, French Massif Central, *Geochimica et Cosmochimica Acta*, 71(5), 1290-1311.

Wittig, N., D. G. Pearson, S. Duggen, J. A. Baker, and K. Hoernle (2010), Tracing the metasomatic and magmatic evolution of continental mantle roots with Sr, Nd, Hf and Pb isotopes: A case study of Middle Atlas (Morocco) peridotite xenoliths, *Geochimica Et Cosmochimica Acta*, 74(4), 1417-1435.

Woodhead, J. D., and C. W. Devey (1993), Geochemistry of the Pitcairn seamounts, I: source character and temporal trends, *Earth and Planetary Science Letters*, 116(1-4), 81-99.

Workman, R. K., and S. R. Hart (2005), Major and trace element composition of the depleted MORB mantle (DMM), *Earth and Planetary Science Letters*, 231, 53-72.

Workman, R. K., S. R. Hart, M. Jackson, M. Regelous, K. Farley, J. Blusztajn, M. Kurz, and H. Staudigel (2004), Recycled metasomatized lithosphere as the origin of the Enriched Mantle II (EM2) end - member: Evidence from the Samoan Volcanic Chain, *Geochemistry, Geophysics, Geosystems*, 5(4), doi: 10.1029/2003GC000623.

Wysoczanski, R., J. Gamble, P. Kyle, and M. Thirlwall (1995), The petrology of lower crustal xenoliths from the Executive Committee Range, Marie Byrd Land volcanic province, West Antarctica, *Lithos*, 36(3-4), 185-201.

Zartman, R. E., P. D. Kempton, J. B. Paces, H. Downes, I. S. Williams, G. Dobosi, and K. Fural (2013), Lower-crustal xenoliths from Jurassic kimberlite diatremes, Upper Michigan (USA): Evidence for Proterozoic Orogenesis and plume magmatism in the lower crust of the Southern Superior Province, *Journal of Petrology*, 54, 575-608.

Zhao, S., and W. Guo (2019), Crustal Structure of Eastern North Carolina: Piedmont and Coastal Plain, *Bulletin of the Seismological Society of America*, 109(6), 2288-2304.

Table 1. Locations and characteristics of samples analyzed for this study, where available.

Sample name	Location description	Latitude (°N)	Longitude (°W)	Outcrop	Reference
<u>Carolinas and Southern ENA:</u>					
CS9	Georgia	34° 45' 21"	83° 29' 33"	Dike	Callegaro et al., 2013
CS26	South Carolina	34° 12' 27"	81° 03' 13"	Dike	Callegaro et al., 2013
CS23	South Carolina	34° 38' 53"	80° 31' 02"	Dike	Callegaro et al., 2013
CS28	South Carolina	34° 39' 08"	80° 31' 01"	Dike	Callegaro et al., 2013
CS14	South Carolina	34° 39' 27"	82° 01' 56"	Dike	Callegaro et al., 2013
CS41	North Carolina	34° 56' 14"	79° 49' 15"	Dike	Callegaro et al., 2013
CS48	North Carolina	35° 04' 15"	79° 50' 38"	Dike	Callegaro et al., 2013
CS46	North Carolina	35° 06' 48"	79° 48' 15"	Dike	Callegaro et al., 2013
CS55	North Carolina	35° 45' 48"	79° 02' 47"	Dike	Callegaro et al., 2013
CS57	North Carolina	35° 50' 11"	79° 00' 48"	Dike	Callegaro et al., 2013
CS49	North Carolina	36° 06' 47"	78° 46' 02"	Sill	Callegaro et al., 2013
CS73	Virginia	37° 17' 44"	78° 27' 38"	Dike	Callegaro et al., 2013
<u>Newark basin:</u>					
NEW03	Palisades Sill			Sill	Merle et al., 2014
NEW136C	Palisades Sill, olivine cumulate layer			Sill	Merle et al., 2014
NEW133	Orange Mountain flow	40° 18' 53"	75° 50' 53"	Lava Flow	Merle et al., 2014
NEW68	Preakness flow	40° 38' 50"	74° 34' 23"	Lava Flow	Merle et al., 2014
NEW52	Preakness flow	40° 40' 33"	74° 24' 32"	Lava Flow	Merle et al., 2014
NEW74	Hook Mountain flow	40° 49' 03"	74° 19' 45"	Lava Flow	Merle et al., 2014

Morocco:

AN134	Tiourjdal section, basal flow	31° 07' 40"	7° 20' 46"	Lava Flow	Marzoli et al., 2004
-------	-------------------------------	-------------	------------	-----------	----------------------

Sierra Leone:

SL45	High-TiO ₂ sample, Freetown Layered Complex, Sierra Leone				Callegaro et al., 2017
------	----------------------------------------------------------------------	--	--	--	------------------------

Table 2. Hafnium isotope measurements for samples analyzed in this study.

Sample name	Lu (ppm) *	Hf (ppm) *	$^{176}\text{Hf}/^{177}\text{Hf}$	$2s^{**}$	eHf a	$^{176}\text{Hf}/^{177}\text{Hf}_{201}$ Ma	eHf, 201 Ma a
<u>Carolinas and Southern ENA:</u>							
CS9	0.51	2.02	0.282879	0.000004	3.34	0.282745	3.02
CS26	0.45	1.61	0.282762	0.000004	-0.81	0.282613	-1.64
CS23	0.40	1.68	0.282908	0.000004	4.33	0.282782	4.33
CS28	0.35	1.17	0.282839	0.000003	1.93	0.282683	0.83
CS14	0.42	1.77	0.282753	0.000004	-1.14	0.282626	-1.16
CS41	0.32	0.94	0.282880	0.000004	3.35	0.282698	1.35
CS48	0.35	1.13	0.282826	0.000003	1.47	0.282664	0.17
CS46	0.43	2.54	0.282835	0.000004	1.76	0.282745	3.03
CS55	0.47	1.74	0.282960	0.000002	6.20	0.282818	5.62
CS57	0.37	1.11	0.282883	0.000004	3.46	0.282706	1.65
CS49	0.34	1.33	0.282962	0.000003	6.26	0.282825	5.86
CS73	0.38	1.54	0.282568	0.000003	-7.67	0.282437	-7.85
<u>Newark basin:</u>							
NEW03	0.29	2.95	0.282727	0.000002	-2.06	0.282674	0.53
NEW136C	0.20	1.54	0.282743	0.000004	-1.47	0.282673	0.50
NEW133	0.23	2.37	0.282754	0.000002	-1.11	0.282702	1.50
NEW68	0.25	2.22	0.282849	0.000002	2.26	0.282789	4.57
NEW52	0.35	2.07	0.282794	0.000004	0.32	0.282704	1.58
NEW74	0.62	3.00	0.282930	0.000002	5.13	0.282821	5.71

Morocco:

AN134

0.31 3.66 0.282769 0.000002 -0.57 0.282724 2.27

Sierra Leone:

SL45

0.05 0.16 0.282917 0.000005 4.67 0.282785 4.45

* Lutetium and Hf elemental compositions from Callegaro et al. (2013, 2017), Marzoli et al. (2004), and Merle et al. (2013).

** Uncertainties for $^{176}\text{Hf}/^{177}\text{Hf}$ measurements reported as 2s standard errors.

a eHf values for measured results calculated using a CHUR $^{176}\text{Hf}/^{177}\text{Hf}$ ratio of 0.282785. Age-corrected eHf values for 201 Ma were calculated using an adjusted CHUR $^{176}\text{Hf}/^{177}\text{Hf}$ ratio of 0.282659.

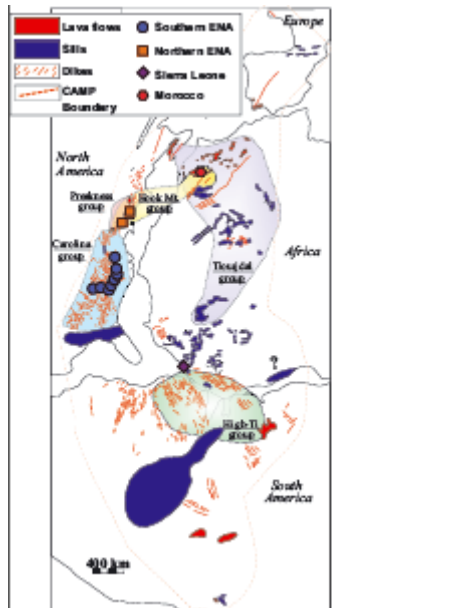


Figure 1. Tectonic reconstruction of the central Atlantic region around the time of CAMP emplacement, with Southern and Northern ENA, Morocco, and Sierra Leone sample locations for this study indicated. Lines and fields in red and blue show the locations of CAMP intrusions and lava flows, as indicated in the legend (after Deckart et al., 2005, Marzoli et al., 2018). Indicated groupings within CAMP refer to magma categories defined by Marzoli et al. (2018).

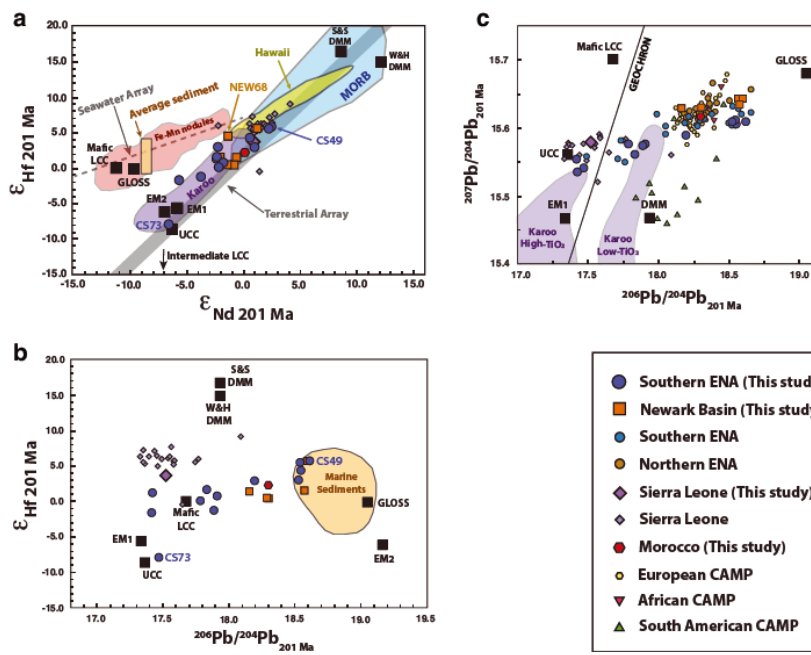


Figure 2. Age-corrected isotope results for samples analyzed in this study, with comparative values from the literature, for **a.** $\epsilon_{\text{Hf}} 201\text{Ma}$ vs. $\epsilon_{\text{Nd}} 201\text{Ma}$, **b.** $\epsilon_{\text{Hf}} 201\text{Ma}$ vs. $^{206}\text{Pb}/^{204}\text{Pb}_{201\text{Ma}}$, and **c.** $^{207}\text{Pb}/^{204}\text{Pb}_{201\text{Ma}}$ vs. $^{206}\text{Pb}/^{204}\text{Pb}_{201\text{Ma}}$. Lead and $\epsilon_{\text{Nd}} 201\text{Ma}$ isotope data for samples in this study are from Callegaro et al. (2013, 2017) and Merle et al. (2014). Other literature data for CAMP are from Callegaro et al. (2013, 2014, 2017), Deckart et al. (2005), Jourdan et al. (2003), Marzoli et al. (2019), Merle et al. (2011, 2014), and Whalen et al. (2015), with regional groups defined after Whalen et al. (2015). End members are shown as black squares, with values as in Table S1 and described in the text; “GLOSS” refers to global average subducted sediment after Plank and Langmuir (1998) and Chauvel et al. (2008), aged 170 Ma to represent Paleozoic subducted sediments (that is, assuming a subduction recycling age of ~ 370 Ma sampled by CAMP melting at ~ 200 Ma, after Callegaro et al. (2013) and Whalen et al. (2015)), “UCC” refers to the average composition of upper continental crust from the Carolina terrane, “Mafic LCC” and “Intermediate LCC” refer to Proterozoic mafic and intermediate- SiO_2 lower continental crust compositions, as described in the text and Table S2, and the “Geochron” line shows the composition of the geochron corrected to an age of 201 Ma. Also shown for reference are the ϵ_{Hf} vs. ϵ_{Nd} mantle array (Vervoort et al., 2011), the field of MORB (Chauvel et al., 2008), the field of Hawaiian lavas (Blichert-Toft et al., 1999), the global seawater array and the field of ferromanganese nodules (after Albarede et al., 1998), average marine sediments from Chauvel et al. (2014) and Plank and Langmuir (1998), and the field of Karoo LIP basalts (Jourdan et al., 2007), which exhibits a shallow sloping trend similar to Hawaiian basalts and our ENA CAMP array. The composition of average Atlantic OIB is after Marzoli et al. (2019) and references therein, e.g. Cape Verde data from Holm et al. (2006) and Canary Islands data from Klügel et al. (2017). Data sets and compositions unrelated to CAMP are plotted for reference and have not been age-corrected, except where indicated in the text or data tables. End-member, age-corrected isotopic compositions for EM-1, EM-2, and DMM were calculated using the compositions shown in Table S1.

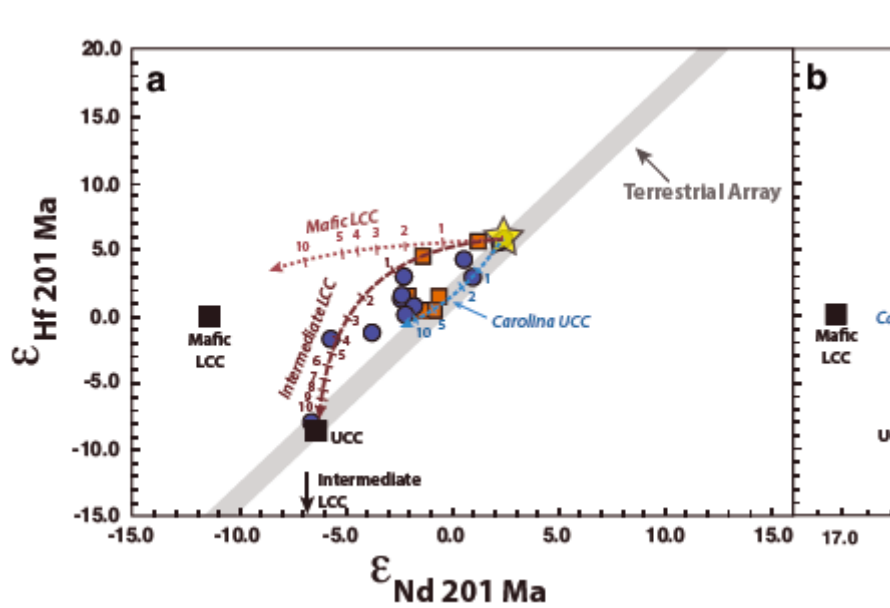


Figure 3. **a.** $\epsilon_{\text{Hf } 201 \text{ Ma}}$ vs. $\epsilon_{\text{Nd } 201 \text{ Ma}}$ and **b.** $\epsilon_{\text{Hf } 201 \text{ Ma}}$ vs. $^{206}\text{Pb}/^{204}\text{Pb}_{201 \text{ Ma}}$ diagrams for samples from this study, showing calculated EC-AFC trajectories after Bohrsen and Spera (2001) and Spera and Bohrsen (2001), as described in the text and using values from Table S1. Trajectories are shown for a parent basalt composition similar to sample CS49, which has the most incompatible element depleted composition based on radiogenic isotope compositions (yellow star; Table 2), with hypothesized compositions for several upper and lower continental crust assimilants described in the text and shown in Table S2. The assimilants shown are 1) averaged Carolina terrane upper continental crust (“Carolina UCC”); 2) a Proterozoic lower crustal mafic granulite (“Mafic LCC”); and 3) an intermediate lower continental granulite with a hypothesized $^{206}\text{Pb}/^{204}\text{Pb}_{201 \text{ Ma}}$ ratio of 17.3, after the discussion in the text (“Intermediate LCC”). Upper continental crust was calculated using mean compositions of measured Carolina terrane crustal rocks from Pettingill et al. (1984) and Sinha et al. (1996) and the data compilation of Whalen et al. (2015). Carolina terrane crustal data set lacks hafnium isotope measurements, so UCC $\epsilon_{\text{Hf } 201 \text{ Ma}}$ values were then calculated assuming a relationship with $\epsilon_{\text{Nd } 201 \text{ Ma}}$ along the terrestrial array (Vervoort et al., 1999) (Table S1). The Proterozoic mafic granulite shown has elevated Lu/Hf ratios, similar to average mafic xenoliths from Michigan (Zartman et al., 2013) and representative of mafic LCC with decoupled ϵ_{Hf} and ϵ_{Nd} . In panel (b), we additionally test mafic LCC with an alternative Pb isotope composition more closely resembling comparable mafic granulite xenoliths from Markt, South Africa (Huang et al., 1995) (“Markt LCC”). Intermediate granulites may have isotopic signatures that record higher time-integrated incompatible element concentrations than mafic basement (i.e., less radiogenic $^{143}\text{Nd}/^{144}\text{Nd}$ and $^{176}\text{Hf}/^{177}\text{Hf}$ ratios), so the intermediate LCC composition has a relatively incompatible element-enriched composition within the range of xenolith measurements by Schmitz et al. (2004). For our intermediate-SiO₂ granulite composition, we also determined partitioning behavior using mineral modes similar to the intermediate-SiO₂ xenolith sampled by Zartman et al (2013). Tickmarks indicate the percentage of crustal assimilant added to the magma, up to a maximum of 10% addition. All other symbols and lines as in Figure 2.

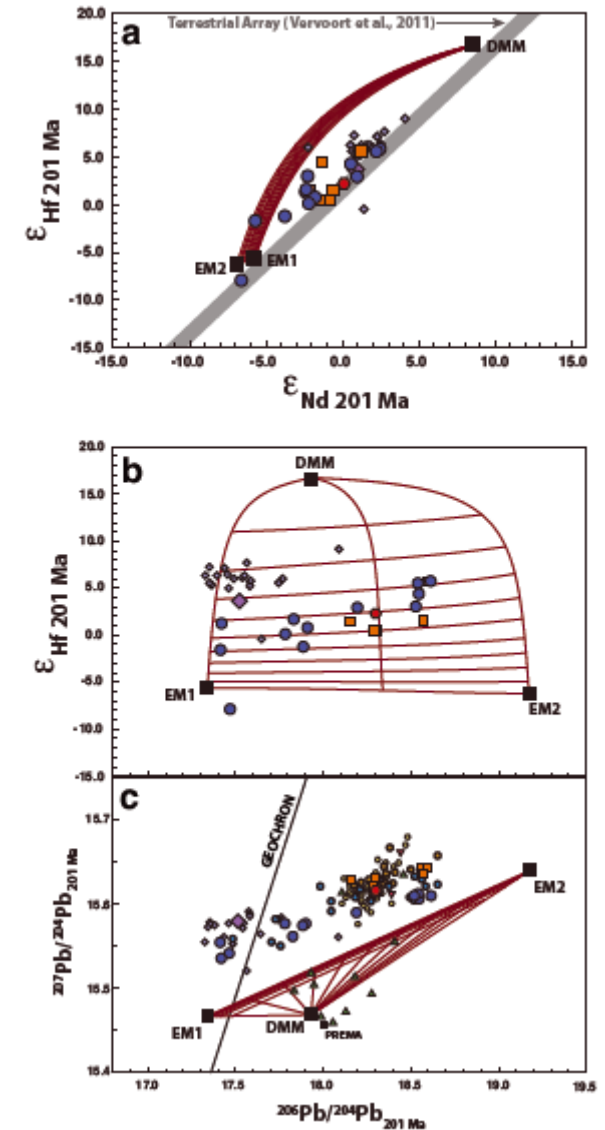


Figure 4. Ternary mixing diagrams for partial melts of DMM, EM-1, and EM-2 sources, as defined in Table S1 and the text, for a. $\epsilon_{\text{Hf } 201\text{Ma}}$ vs. $\epsilon_{\text{Nd } 201\text{Ma}}$, b. $\epsilon_{\text{Hf } 201\text{Ma}}$ vs. $^{206}\text{Pb}/^{204}\text{Pb}_{201\text{Ma}}$, and c. $^{207}\text{Pb}/^{204}\text{Pb}_{201\text{Ma}}$ vs. $^{206}\text{Pb}/^{204}\text{Pb}_{201\text{Ma}}$. Mixing lines are plotted in 10% increments; symbols, lines, and mixing reservoirs as in Figure 2. Mantle reservoirs used for the mixing calculations use relatively recent estimates for the isotopic composition of enriched mantle sources (e.g., Jackson and Dasgupta, 2008; Jackson et al., 2007), resulting in different values than prior studies; however, the results confirm that mixing of these reservoirs fails to explain southern ENA CAMP (Callegaro et al., 2013). More recent research (e.g., Marzoli et al., 2019) suggests that CAMP asthenosphere was in fact less depleted than global DMM and may more closely resemble the PREMA reservoir (Zindler and Hart, 1986), but our mixing trajectories show that the enriched melting end-members are mainly responsible for the observed mismatch, not the depleted end-member.

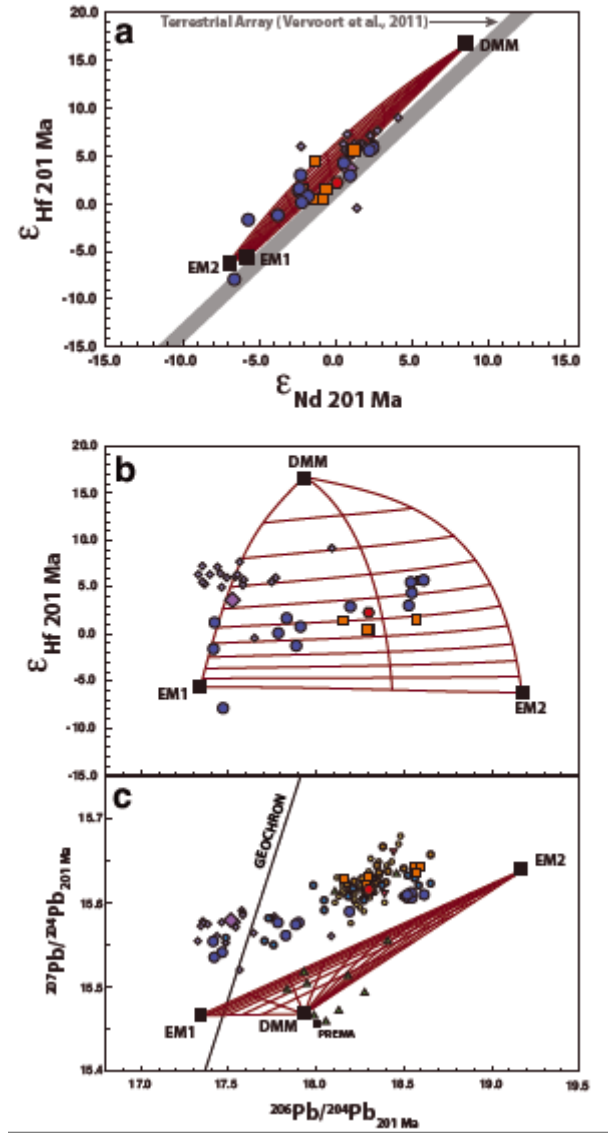


Figure 5. Ternary mixing diagrams for solid DMM, EM-1, and EM-2 source reservoirs, as defined in Table S1 and the text, for a. $\epsilon_{\text{Hf } 201 \text{ Ma}}$ vs. $\epsilon_{\text{Nd } 201 \text{ Ma}}$, b. $\epsilon_{\text{Hf } 201 \text{ Ma}}$ vs. $^{206}\text{Pb}/^{204}\text{Pb}_{201 \text{ Ma}}$, and c. $^{207}\text{Pb}/^{204}\text{Pb}_{201 \text{ Ma}}$ vs. $^{206}\text{Pb}/^{204}\text{Pb}_{201 \text{ Ma}}$. Mixing lines are plotted in 10% increments; symbols, lines, and mixing reservoirs as in Figure 2.

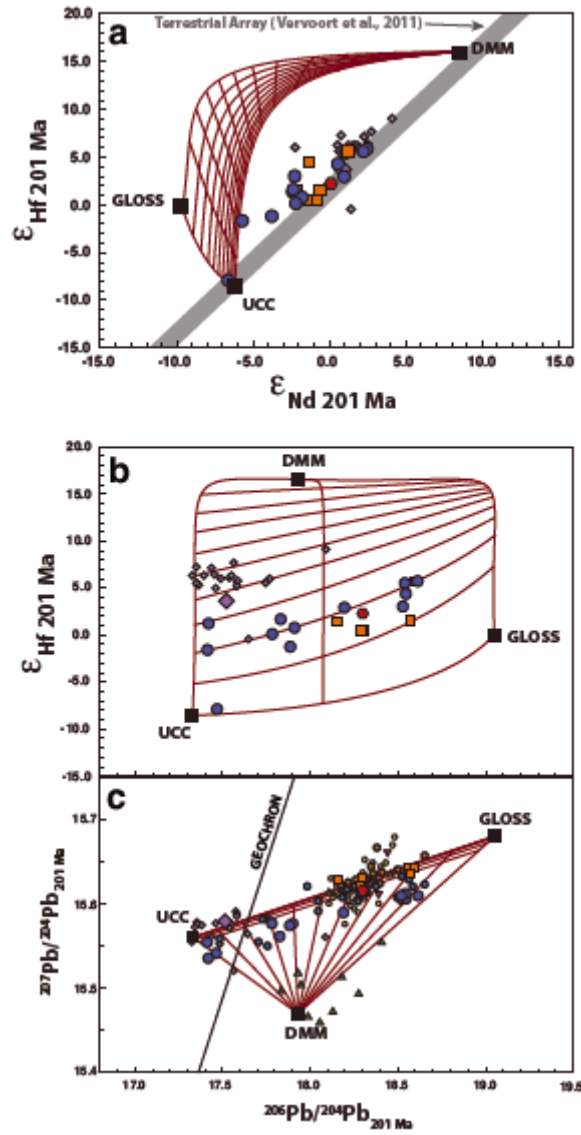


Figure 6. Ternary mixing diagrams for DMM melts, average Carolina terrane continental crust, and average subducted pelagic marine sediments (GLOSS), as defined in Table S1 and the text, for **a.** $\epsilon_{\text{Hf } 201 \text{ Ma}}$ vs. $\epsilon_{\text{Nd } 201 \text{ Ma}}$, **b.** $\epsilon_{\text{Hf } 201 \text{ Ma}}$ vs. $^{206}\text{Pb}/^{204}\text{Pb}_{201 \text{ Ma}}$, and **c.** $^{207}\text{Pb}/^{204}\text{Pb}_{201 \text{ Ma}}$ vs. $^{206}\text{Pb}/^{204}\text{Pb}_{201 \text{ Ma}}$. Mixing lines are plotted in 10% increments; other symbols, lines, and mixing reservoirs as in Figure 2.

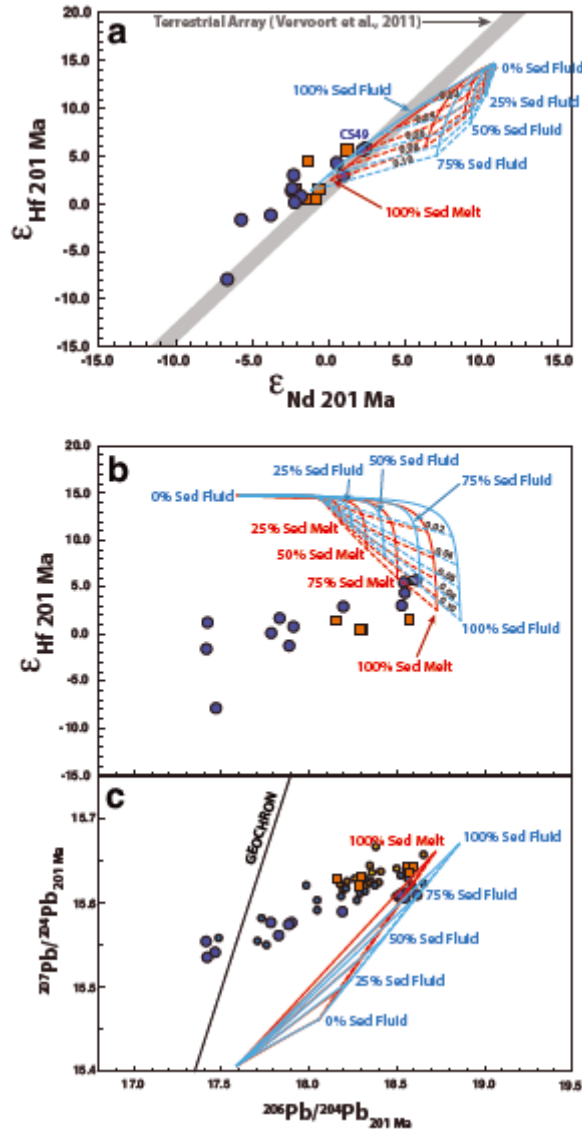


Figure 7. Isotope diagrams showing results of isotopic evolution and partial melting calculations for modified mantle wedge, for **a.** $\epsilon_{\text{Hf } 201 \text{ Ma}}$ vs. $\epsilon_{\text{Nd } 201 \text{ Ma}}$, **b.** $\epsilon_{\text{Hf } 201 \text{ Ma}}$ vs. $^{206}\text{Pb}/^{204}\text{Pb}_{201 \text{ Ma}}$, and **c.** $^{207}\text{Pb}/^{204}\text{Pb}_{201 \text{ Ma}}$ vs. $^{206}\text{Pb}/^{204}\text{Pb}_{201 \text{ Ma}}$ and with symbols and lines as in Figure 2. The trajectories shown indicate calculated mantle compositions for a crustal recycling subduction and metasomatism age of 370 Ma and subsequent mantle melting at 201 Ma. Blue solid lines indicate mantle compositions when metasomatized by a mixture of fluid derived from altered oceanic crust (AOC) and fluid derived from subducted global oceanic sediment; “% Sed Fluid” labels indicate the percentage of sediment-derived fluid in the metasomatizing fluid mixture. Red solid lines indicate the same, but for AOC-derived fluid and sediment-derived partial melts (with corresponding “% Sed Melt” labels). Dashed lines and associated labels indicate the amount of fluid added to the mantle during metasomatism up to 10% addition, as a mass fraction relative to the initial mantle material (0.01 to 0.10). We note that all fractions of added fluid from 1-10% addition are compressed into a single narrow zone in panel c and so are not labeled. See Table S4 for additional modeling details.

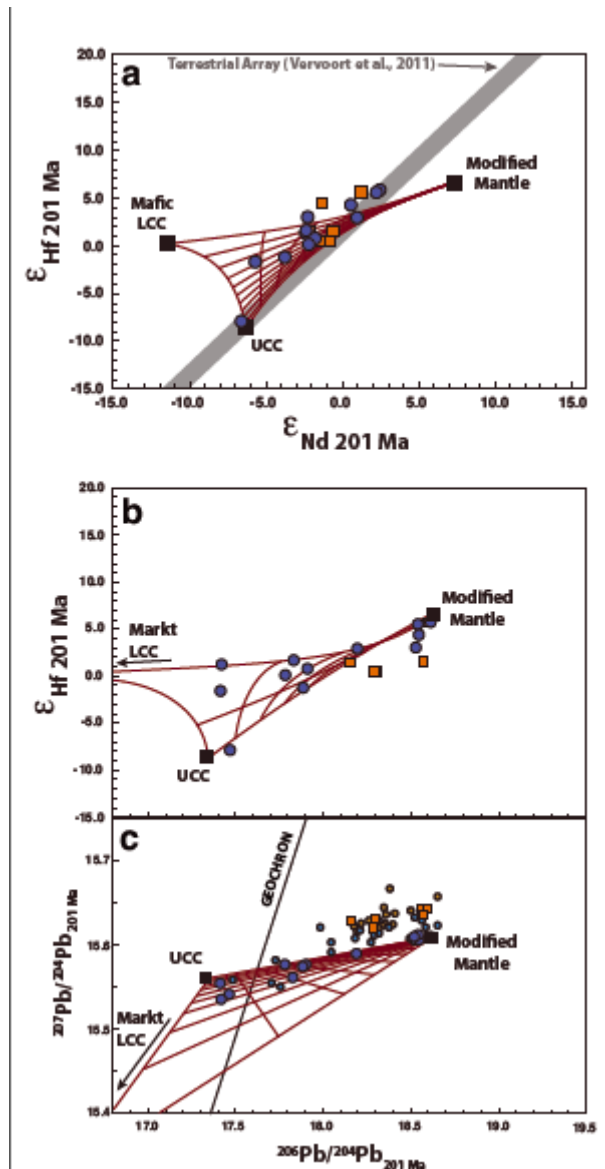


Figure 8. Diagrams showing mixing trajectories between recycled continental crustal rocks and partial melts of modified, metasomatized mantle, for **a.** $\epsilon_{\text{Hf}} 201 \text{ Ma}$ VS. $\epsilon_{\text{Nd}} 201 \text{ Ma}$, **b.** $\epsilon_{\text{Hf}} 201 \text{ Ma}$ VS. $^{206}\text{Pb}/^{204}\text{Pb}_{201 \text{ Ma}}$, and **c.** $^{207}\text{Pb}/^{204}\text{Pb}_{201 \text{ Ma}}$ VS. $^{206}\text{Pb}/^{204}\text{Pb}_{201 \text{ Ma}}$ and with mixing lines in 10% increments and all other symbols as in Figure 2. The “modified mantle” mixing end member is a calculated 6% batch melt of mantle metasomatized using the methods described in the text and shown in Figure 7 and Table S4. The example case shown is for mantle modified by 7% addition of a fluid derived 25% from AOC and 75% from subducted sediments, with a 370 Ma recycling age and 201 Ma melting age. The UCC composition shown is local Carolina terrane, and the LCC composition is the “Markt mafic granulite” composition, both from Table S1.